SMALL ANGLE NEUTRON SCATTERING STUDY OF GLOBULAR PROTEINS CONFINED IN POROUS CARBONS

Balázs Nagy,[1] Ajna Tóth,[1] Irina Savina,[2] Sergey Mikhalovsky,[2,3] Lyuba Mikhalovska,[2] Isabelle Grillo,[4] Erik Geissler,[5] Krisztina László[1*]

[1]Department of Physical Chemistry and Materials Science, Budapest University of Technology and Economics, H-1521 Budapest, Hungary

[2]School of Pharmacy and Biomolecular Sciences, University of Brighton, Brighton, BN2 4GJ, United Kingdom

[3]School of Engineering, Nazarbayev University, Astana, 010000, Republic of Kazakhstan

[4]Institut Laue Langevin, 71 avenue des Martyrs - CS 20156 - 38042 Grenoble Cedex 9, France

[5]Université Grenoble Alpes and CNRS, LIPhy, F-38000 Grenoble, France

Abstract

This article reports measurements of the concentration distribution of two model proteins adsorbed from aqueous solution by two different high surface area carbons, using small angle neutron and X-ray scattering (SANS and SAXS). The proteins investigated were bovine serum albumin (67 kDa), and bovine pancreatic trypsin inhibitor (BPTI), also known under the name aprotinin (6.5 kDa). The two carbon substrates were C1, an open structured carbon aerogel derived from a resorcinol–formaldehyde polymer aerogel, and C2, a commercial nanoporous carbon from

*Corresponding author. E-mail: *klaszlo@mail.bme.hu

MAST Carbon (UK). Although both C1 and C2 possess a high proportion of pores that are either closed or inaccessible to low temperature nitrogen vapour, the size distribution of the accessible pores is broad enough to accommodate BSA molecules. In C1, which is hydrophobic, the BSA molecules migrate individually into pores that are compatible with their size, whereas BPTI forms clusters having the same size as BSA. With C2, the hydrophilic internal surface limits the adsorption efficiency. The strong adhesion of proteins to hydrophilic surfaces prevents diffusion of either molecule into the micro- and nanopores. In this sample both BSA and BPTI form large clusters. These observations have relevance in biomedical applications, such as haemoperfusion or as a medium for protein storage.

1. Introduction

The way in which biomolecules adsorb and migrate on solid surfaces, notably on porous substrates, is the focus of converging interests from investigations into protein conformation, [1-4] physical adsorption processes,[5,6,7] and medical applications.[8,9] Activated carbons are a class of porous substrates that have been widely employed for many centuries as general adsorbents. They are also invaluable as adsorbents of small molecules in numerous applications related to public health, such as drinking water purification, personnel protection, etc. More recently their range of uses has extended to medical applications, notably for purification of bio-fluids. Treatment of patients suffering from acute poisoning, drug overdose, hepatic coma, or metabolic disturbances removes toxins from the bloodstream by circulating the patient's blood through an adsorbent, usually activated carbon or resins. Such haemoperfusion procedures extract small to medium sized molecules that tend to be more difficult to remove by conventional haemodialysis. The adsorbent material may

be coated or immobilized to prevent fine particles from entering the patient's blood. [8,9] In such applications the size of the adsorbent pores relative to that of the target toxin is of critical importance, as many toxins are proteins of a size that excludes them from micropores. Carbons with larger pore size are required.

Adsorption techniques yield overall information on the amount of a target molecule adsorbed in a substrate, but say little about how the molecules are distributed inside it. By contrast, small angle X-ray scattering (SAXS),[10] and more particularly small angle neutron scattering (SANS),[11,12] are non-destructive techniques that can detect the spatial structure and organisation of molecules adsorbed inside a porous medium.[5] Such studies are of particular interest for biomolecules, where the conformation is not necessarily the same as in solution. In applications involving extraction and storage of proteins, for example, little is known of how associative behaviour or the uptake and release mechanisms affect the mobility of the adsorbate and the retention capacity of the porous medium.[5] For a fuller understanding of how a model protein is adsorbed in porous carbons of different pore size distribution, different surface chemistry and different hydrophobicity, both approaches are desirable. For clarity, this account is separated into two parts: the first part is a companion article [13], which describes the macroscopic adsorption measurements. The present paper focuses on the scattering results.

2. Experimental

2.1. Materials

Two porous carbons were studied: a carbon aerogel (C1), obtained from the resorcinol-formaldehyde polycondensation reaction [12,14], and a commercial medical grade porous carbon prepared from phenol formaldehyde resin (C2) (MAST

Carbon, UK) [15-17]. Neither sample C1 nor sample C2 was coated. The probe proteins were bovine serum albumin (BSA, molecular weight 66.1 kDa) supplied by Calbiochem, and bovine pancreatic trypsin inhibitor (BPTI, molecular weight 6.5 kDa), also known under the name aprotinin (Sigma-Aldrich). The solubility of BSA in deionized water is 40 g/L.[1] BPTI is also soluble both in H_2O and D_2O at 20ºC (>30 g/L).[18] For the SANS measurements stock protein solutions at 10 g/L were prepared on site at the Institut Laue-Langevin in 99.7% D_2O with no added buffer. The pH of the stock solution, measured with a pH meter, was 6.9. The value of pD is accordingly pD= 6.9+0.4= 7.3.[19] For the SANS measurements on BSA in acid conditions, 7.5 mL of the stock solution and its pH were adjusted to ~2.8 (pD=3.2) by adding 10 µL of a tenfold diluted solution of DCl in D_2O.

2.2. Adsorption measurements

The principal characteristics of the carbons obtained from the nitrogen adsorption isotherms at -196 °C [13] are reproduced in the tables below. **Table 1** lists the surface area S_{SAS} measured in the present work by SANS and SAXS, together

Table 1. Measurements from SAS, nitrogen adsorption and pycnometry [13]

Sample	S_{SAS} [a]	S_{BET}	V_{tot}	$V_{0.95}$ [b]	V_{μ}	d_C [c]	pH
	m^2/g		cm^3/g			g/cm^3	
C1	1784	847	1.69	0.80	0.34	0.075	8.6
C2	2630	1248	1.27	0.96	0.50	0.44	6.6

[a] see Supplementary Information, [b] $V_{0.95}$: pore volume at p/p_0=0.95; [c] macroscopic density from He pycnometry.

[1] https://www.sigmaaldrich.com/content/dam/sigma-aldrich/docs/Sigma/Product_Information_Sheet/a4919pis.pdf (retrieved 15/04/2016)

with the apparent surface area S_{BET} calculated from the BET model [20]. The total pore volume (V_{TOT}) was derived from the amount of vapour adsorbed at $p/p_0 \rightarrow 1$, assuming that the pores are then filled with liquid adsorbate. Similarly, the pore volume was determined at $p/p_0 = 0.95$ ($V_{0.95}$), just before the sharp increase of the isotherms. The micropore volume V_{μ} was determined using the Dubinin-Raduskevich (DR) model [21]. The pore size distribution (PSD) was calculated using quenched solid density functional theory (QSDFT) [22]. Slit pores were assumed. **Table 2** shows the incremental surface areas and volumes deduced from these models.

Table 2. Incremental surface area $S=S_{BET}-S_d$ and pore volume $V=V_{total}-V_d$

	BSA			BPTI	
	C1		C2	C1	C2
	unbuffered pH 6.9	pH3	unbuffered pH 6.9		
limiting pore width[a] (Å)	40	40	40	24.2	24.2
S (m^2/g)	203	203	105	279	125
V (cm^3/g)	1.20	1.20	0.87	1.41	0.80

[a] smallest effective dimension of the free protein, or cluster (Supplementary Information)

2.3. Methods: SANS and SAXS

The SANS measurements were made on the D11 instrument at the Institut Laue Langevin, Grenoble, at incident wavelength λ=7.8 Å, with wavelength spread $\Delta\lambda/\lambda$=0.1. The carbon samples were powdered and placed in contact with either D_2O

or the protein solution in D_2O. Both protein solutions were prepared in 99.7% D_2O at concentration 10 g/L, without buffer or added salt. The conditions applied here were identical to those in the uptake measurements in the saturation range of the isotherms.[13] After incubation overnight prior to the measurement the slurries were transferred to flat quartz cells of 2 mm path length. The dry carbon powders were contained in 1 mm quartz cells.

Since the intensity of the amorphous scattering peak of water at 2.0 $Å^{-1}$ defines the amount of water present in the samples, measurements at wider angles were also made on the D16 instrument at wavelength 4.74 Å. For this instrument, the samples were contained in cylindrical low boron content glass cells of outer diameter 5 mm. Corrections for incoherent scattering were made using the expression [23]

$$I(q)= I_s(q)/T_s - I_b(q)T_s(1\text{-}T_b)/[T_b(1\text{-}T_s)] \quad (1)$$

where $I(q)$, $I_s(q)$ and $I_b(q)$ are the normalized scattering intensities of the total signal, of the sample and of the background, respectively, and where T_s and T_b are the corresponding transmission factors. (Expression (1) is recommended in SANS measurements, where attenuation of the incident beam occurs through scattering, in contrast to SAXS, where the attenuation is dominated by absorption.) Intensities were normalised with respect to a standard detector calibration supplied by the Institut Laue-Langevin. In Eq. 1, q is the transfer wave number $q=(4\pi/\lambda)\sin(\theta/2)$, λ is the incident wavelength and θ is the scattering angle.

SAXS measurements, made at the French CRG beam line BM02 of the European Synchrotron Radiation Facility, Grenoble, were used as a reference to estimate the incoherent neutron scattering intensity from the dry carbon samples.

3. Results and discussion

3.1. Bulk protein solutions

3.1.1. BSA

The conformation of BSA is sensitive to external conditions such as pH [24,25]. Below pH 4.7, the isoelectric point of BSA,[2] the electrostatic interactions force the molecule into an extended shape. In this investigation the measurements on BSA were conducted at pH 6.9, as well as at pH 2.8.

Figure 1 shows the SANS response of bulk solutions of BSA in D_2O at pH 6.9. In dilute solutions of neutral polymers the low q response can usually be approximated by the Debye expression for the scattering intensity from particles of radius of gyration R_G,

$$I(q)=I(0)\exp[-(qR_G)^2/3] \quad (2)$$

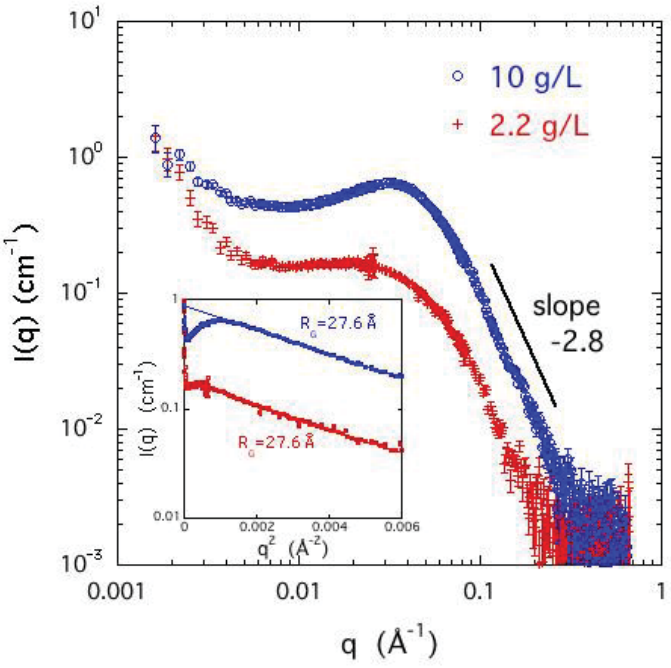

Figure 1. SANS response of BSA in D_2O at pH 6.9, after subtraction of the D_2O signal. The maxima are due to residual electrostatic repulsion in the salt-free solutions. Inset: Guinier plot of the SANS response from the 10 g/L and 2.2 g/L solution of BSA (lower data set). In both cases the radius of gyration is R_G = 27.6 Å.

The difference between the experimental curves in the intermediate wave vector range q of Fig. 1 and the monotonic variation expressed in Eq. 2 stems from electrostatic repulsion between the molecules. The repulsion gives rise to interparticle structure in the form of a correlation peak, the position of which, q_{max}, defines the mean distance of separation between the proteins, $d \approx 2\pi/q_{max}$. When d is larger than the outer diameter of the coil $2R$ (i.e., non overlapping conditions), q_{max} varies with the concentration c as $c^{1/3}$[26]. (For simplicity, in this paper we represent the protein shape as a solid sphere, for which $R=(5/3)^{1/2}R_G$.) With decreasing concentration the correlation peak disappears and the response in the region $qR_G<1$ reverts to Eq 2. At very low q, additional scattering may arise due to a small fraction of larger clusters in the solution.

To minimise the principal effects of the interparticle structure [27, 28], and for consistency with the measurements of the proteins adsorbed inside the carbons, we apply Eq. 2 to the data in the q-range above q_{max} taken from the region $1 \leq qR_G \leq 2$. The inset of Figure 1 displays the data in the Guinier representation $\log[I(q)]$ *vs* q^2. This representation yields acceptable fits both for the 10 g/L and the 2.2 g/L BSA solutions. The identical values obtained for the two concentrations, R_G=27.6 Å, are also consistent with measurements reported in the literature [29– 31]. If we assume the globular BSA molecules to be uniform spheres of external radius R, then R=35.6 Å, which, in spite of the oversimplification of the uniform sphere model, is in reasonable agreement with the measured hydrodynamic radius of BSA, R_H =34.8 Å. [32] We recall that in measuring R_G the range of q in the Guinier approximation is generally stated to be $qR_G \leq 1$. In practice, the range of validity depends on the form factor $P(q)$ of the particle, and can extend well beyond this limit. [33] To access the information below the correlation peak, we adopt the separability approximation for

the scattered intensity

$$I(q)= S(q)\, P(q) \tag{3}$$

together with the expression for the structure factor due to Posselt et al. [34]

$$S(q)=1/\{1+3p[\sin(qD)-qD\cos(qD)]/(qD)^3\} \tag{4}$$

where p is a parameter that describes the strength of the interparticle repulsion and D is the mean interparticle distance. With D=140 Å and 232 Å respectively for the 10 g/L and 2.2 g/L BSA solutions, the Guinier representation of $P(q)= I(q)/S(q)$ yields an identical value for R_G in the region $0.24\leq qR_G\leq 1$ to that in the region $1\leq qR_G\leq 2$, shown in the inset of Figure 1.

The extrapolated scattering intensity $I(0)$ in Eq. 2 yields M_W, the weight-average molecular weight of the polymer. For a dilute solution of polymers of mass M_W at concentration c, $I(0)$ is defined by

$$I(0)=K^2 c M_W/N_A \tag{5}$$

where $K^2=(\Delta\rho V_P)^2$ is the neutron scattering contrast between the polymer and the solvent, and N_A is Avogadro's number. V_P is the dry molar volume of the protein, and

$$\Delta\rho=(\rho_{D2O}-\rho_{BSA}) \tag{6}$$

is the difference in scattering length density between the protein and the surrounding D_2O.

According to Nossal et al. [30], for BSA in D_2O at pH=5.53, V_P =0.734 cm^3/g, and the value of $\Delta\rho^2$ is

pH 5.53: $$\Delta\rho^2=13.0\times10^{20}\ cm^{-4} \tag{7}$$

With this value of $\Delta\rho^2$ and the extrapolated intensity $I(0)$=0.85 cm^{-1} from the inset of Figure 1, the apparent molecular weight for the BSA in the 10 g/L solution is

$$M_w = 73\ kDa \tag{8a}$$

Similarly, for the solution at 2.2 g/L, where $I(0)$=0.181 cm^{-1}, Eq. 5 yields

$$M_w = 71 \text{ kDa} \quad (8b)$$

These estimates of M_w are sensitive to the scattering length density ρ_{BSA}. The discrepancy between the results in Eq. 8 and the known molecular weight of BSA, 66.1 kDa, reflects the change in ρ_{BSA} due to ionisation of the protein when the pH exceeds the pKa of the acid groups. (BSA possesses two pKa values, 5.7 and 6.8 [25].) In the protein solution with D_2O, exchangeable protons are replaced by deuterium, and consequently ionisation of the dissolved BSA involves the loss of a deuteron and hence a reduction in the value of ρ_{BSA}. This change increases the contrast $\Delta\rho^2=(\rho_{D2O}-\rho_{BSA})^2$ with respect to the surrounding D_2O. The resulting overestimate of M_w of BSA at pH 6.9 in Eq. 8 can be brought into line with the known molecular weight by resetting $\Delta\rho^2$ to

pH 6.9:
$$\Delta\rho^2 = 72\times13.0\times10^{20}/66.1$$
$$= 14.16\times10^{20} \text{ cm}^{-4} \quad (9)$$

These measurements incidentally imply that in solution the BSA molecules are present as monomers.

At low pH, both the state of ionisation and the conformation of BSA in solution differ from that prevailing at pH 6.9. Earlier measurements by SANS [31] and birefringence [32] showed that at low pH the shape of BSA is elongated.[35, 36] This elongation is the consequence of the protonated (/deuterated) state of the protein that occurs already at moderately low pH, which imposes a proxy polyelectrolyte character on the molecule. The flexibility of the BSA molecule, which stems from its high degree of hydration, allows its conformation to accommodate when the ionic environment is modified.[37] **Figure 2** shows the SANS response of BSA in solution at pH 2.8. The increased radius of gyration (Fig. 2 inset) reflects the elongated conformation. The stretched cylindrical shape gives rise to the reduced slope in the

region $1/L<q<1/r_0$, where L is the length of the cylinder and r_0 its radius, and to the shoulder at $q\approx0.1$ Å^{-1}. The latter feature indicates that the cross-sectional radius r_0 of the cylinder is approximately $1/q\approx10$ Å.

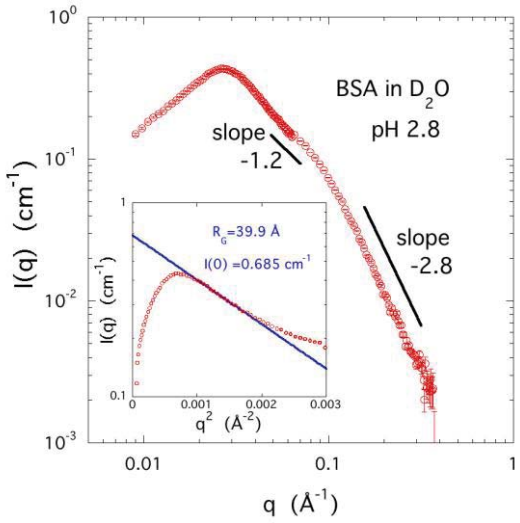

Figure 2. SANS response of 10 g/L solution of BSA in D_2O at pH 2.8, after subtraction of the D_2O signal; inset: Guinier plot of data from the range $0.001\leq q^2\leq0.002$ Å^{-2}.

The Guinier plot in the inset of Figure 2 yields R_G = 39.9 Å and $I(0)$=0.685 cm^{-1} for the extrapolated intensity. With the contrast factor of Eq.6, the resulting mass is M_w = 58.9 kDa, i.e., lower than the known molecular weight. Below the isoelectric point of BSA (pH 4.7) [2], however, the ionisation that occurred at high pH is now reversed: at pH 2.8 deuterons recombine with the acidic groups, thereby enhancing ρ_{BSA} and decreasing $(\rho_{D2O}-\rho_{BSA})^2$. Correction for deuteron condensation on the BSA at pH 2.8 accordingly requires that $\Delta\rho^2$ be reset to

pH 2.8: $\Delta\rho^2=58.9\times13.0\times10^{20}/66.1=11.6\times10^{20}$ cm^{-4} (10)

3.1.2. BPTI

For the lower molecular weight protein BPTI, all SANS measurements were made at pH 6.9. The high isoelectric point (≈10.5) of this molecule [38] implies that in physiological pH conditions its degree of ionization is small. As observed also by Appavou et al. [39], no sign of a correlation peak is visible in the signal from the solution (**Figure 3**), confirming the absence of ionization of this molecule in solution. The radius of gyration (Fig. 3 inset), R_G= 9.8 Å, is somewhat smaller than that reported in ref. [39], where buffer solutions were employed. As the present samples were prepared without buffer, however, adsorption of ions from the solution does not occur and the conditions governing the hydration layer can be different. These measurements thus represent the undecorated BPTI molecule. It is notable that, just as with BSA, the q range in the Guinier representation over which the value of R_G remains constant extends up to qR_G =2.

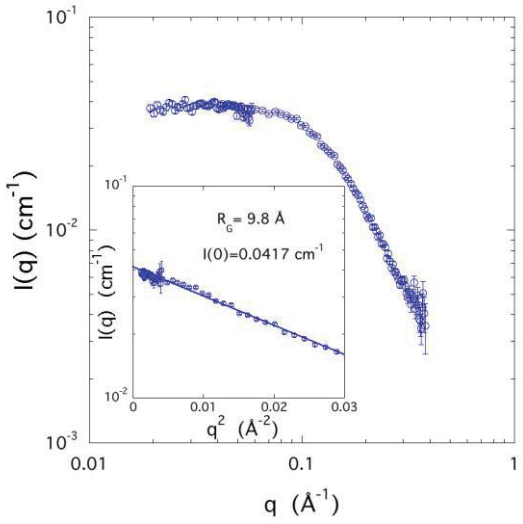

Figure 3. SANS response from a 10 g/L BPTI solution in D_2O. Inset: Guinier plot from the low q region. This system displays no correlation peak.

From the inset of Fig. 3, the extrapolated intensity for the 10 g/L solution is $I(0)$=0.0417 cm^{-1}. Insertion of these values into Eq. 3 yields for the value of K

$$K = 2.03\times10^{10}\ \text{cm/g} \quad (11)$$

This lies close to the average of the range of K values listed in reference [39] observed during the pressure cycle in D_2O. **Table 3** summarizes the values of the contrast factor K for BSA and BPTI.

Table 3: Neutron scattering contrast factor $K=\Delta\rho V_P$ of proteins in D_2O

protein	pH 6.9	pH 5.53	pH 2.8	Acetic acid-D buffer
	(cm/g)			
	this work	[30]	this work	[39]
BSA	2.76×10^{10}	2.65×10^{10}	2.50×10^{10}	-
BPTI	2.03×10^{10}	-	-	$1.72\text{-}2.90\times10^{10}$

3.2. SANS measurements of protein solutions in the carbon matrices

3.2.1. BSA

In the SANS measurements of the two nanoporous carbons in equilibrium with the D_2O solutions of BSA (**Figures 4 and 5**), the scattering length density ρ of the D_2O solvent approximately matches that of the signal from the carbon in the micropore (q > 0.3 Å^{-1}) and mesopore size range (0.01< q < 0.3 Å^{-1}). Since ρ_C and ρ_{D2O} are similar, the intensity $I(q)=(\rho_C-\rho_{D2O})^2S(q)$ is small, where $S(q)$ is the structure factor of the carbon and $(\rho_C-\rho_{D2O})^2$ is the contrast factor between the carbon and the D_2O. At lower q (<0.01 Å^{-1}), however, the signal of the carbons containing D_2O alone displays strong residual scattering with power law behaviour of the form $I(q)\propto q^{-p}$, where the exponent is p=4.0 in C1, and $p\approx3$ in C2. Power law responses with $p\geq3$ are the signature of surface scattering [40,41]. The strong surface scattering feature of C1_D_2O in Fig. 4 arises from a discontinuity in the contrast factor at an interface, i.e.,

a layer between the carbon surface and the D_2O where the value of ρ is smaller than ρ_C. This could either be a material layer with high proton density or a void layer resulting from incomplete wetting of the carbon by the D_2O. The strongly hydrophobic surface of C1, as concluded from the water uptake isotherms [13], points to the latter explanation [40, 41]. Confirmation of this interpretation is found in Fig. 4, which shows how the SANS response changes when BSA is added to the solution: when the proteins adsorb on the walls of the larger pores, the discontinuity in the contrast factor $(\rho_C-\rho)^2$ decreases between the carbon and the medium adjacent to the interface, and the surface scattering feature disappears.

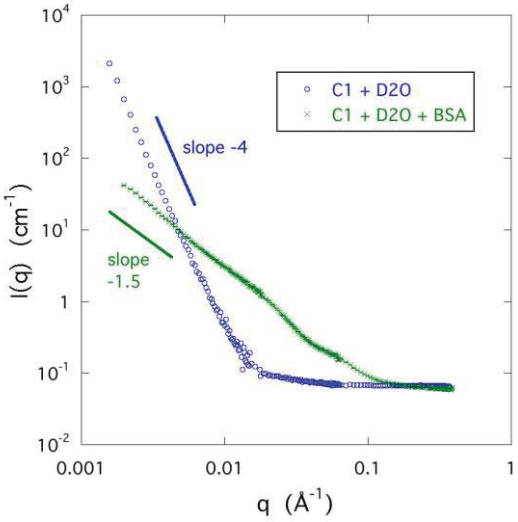

Figure 4. SANS response of carbon aerogel C1 with D_2O alone (o), and same sample with D_2O and BSA at pH 6.9 (×). The flat signal at high *q* is the contribution from D_2O.

Carbon C2 in D_2O alone also displays a steep slope in the low *q* range (**Figure 5**), but its weaker power law slope (-2.95±0.1) lies at the threshold between volume scattering and scattering from very rough surfaces [41]. The low *q* responses of the samples containing BSA also differ qualitatively from those of sample C1: in this case

the protein signal adds to, rather than subtracts from, that of the carbon-water system. In C2, therefore, the contrast mismatch at low q is not the result of poor wetting, as in C1, where, in the contrast factor $(\rho_C-\rho)^2$, $\rho\approx 0$. Instead, it reflects the presence of surface groups associated with protons, which lower the neutron scattering length density. The difference in surface composition of the two carbons is reflected both in the difference of their surface pH (Table 1), and in their water vapour isotherms [13]. C2 exhibits much higher water uptake throughout the isotherm. The surface of C2 is therefore more hydrophilic than that of C1. These observations are consistent with the substantially larger incoherent scattering intensity in the dry C2 sample (0.011 cm^{-1}), an unmistakable indicator of higher hydrogen content.

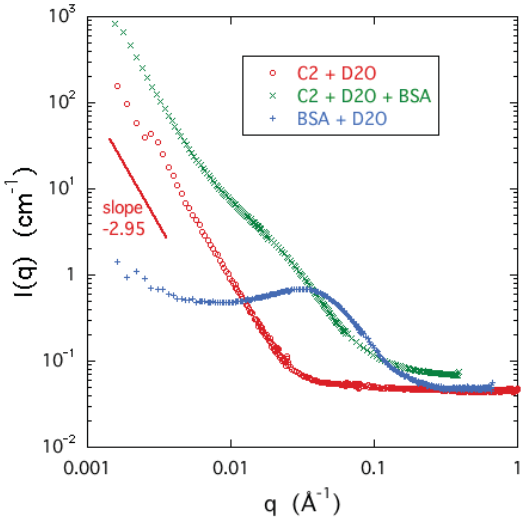

Figure 5. SANS response of sample C2 containing (o): pure D_2O, and (×): BSA in D_2O. The signal from the bulk solution (10 g/L) of BSA in D_2O (+) is shown for comparison. The D_2O signal has not been subtracted from these responses.

Figure 6 shows the scattering signals from BSA in carbon C1 and C2, after subtraction of the response from D_2O. As in the insets of Figures 1-3, the data are plotted in the Guinier representation log$I(q)$ *vs* q^2. Comparison of the values of R_G

obtained from the fits to the data in the region above q_{max} (q>0.01 Å^{-1}) with those in solution indicates that in C1 at pH 6.9 BSA is present as a monomer, while in C2 the much larger radius of gyration is characteristic of aggregates.

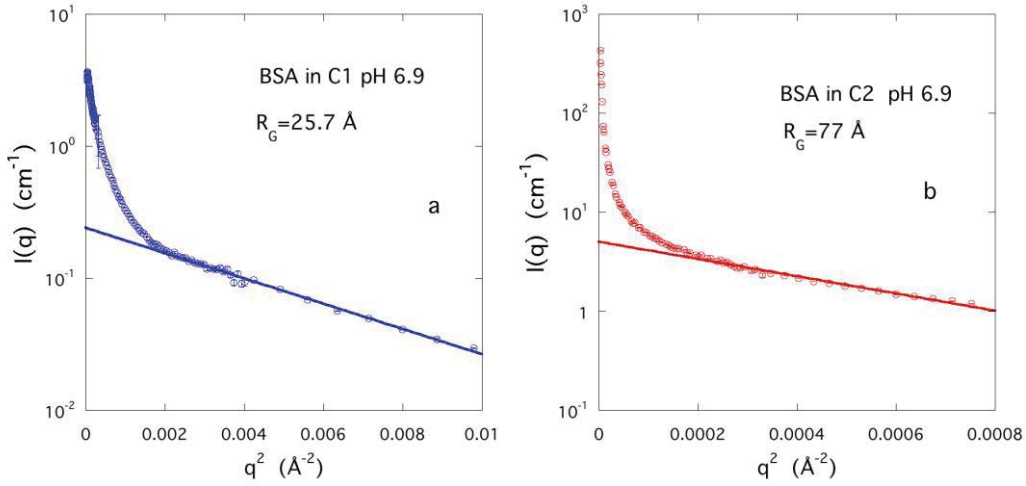

Figure 6. Guinier plots of the scattering intensity $I(q)$ at pH 6.9 (after subtraction of the D_2O signal) in the q-region above q_{max}: (a) BSA in the carbon aerogel C1; (b) in the MAST carbon C2. The extrapolated intensities of these curves are $I(0)$=0.24 cm^{-1} for BSA in C1, and $I(0)$=5.0 cm^{-1} for BSA in C2.

At pH 2.8, the situation is similar. In C1, BSA displays a region of exponential decay in the Guinier representation of **Figure 7a** with a slope corresponding to R_G=24.9 Å, i.e., similar to that at pH 6.9, but notably smaller than in free solution at pH 2.8. Here again, however, the radius of gyration is consistent with BSA in the form of a monomer. In C2, by contrast, the SANS curve appears featureless (**Figure 7b**), being dominated by the power law response at low q. The lower curve in Figure 7b shows the same data after subtraction of the asymptotic power law curve of slope -2.9. Two features are revealed, a broad maximum at q≈0.0065 Å^{-1}, and a weak shoulder at q≈0.026 Å^{-1}. The latter feature possesses a short region that can be analyzed in a Guinier representation (**Figure 7c**). The value found for R_G, 41.8 Å,

however, is significantly larger than in C1. To determine whether this component is a monomer or an oligomer requires an estimate of its mass.

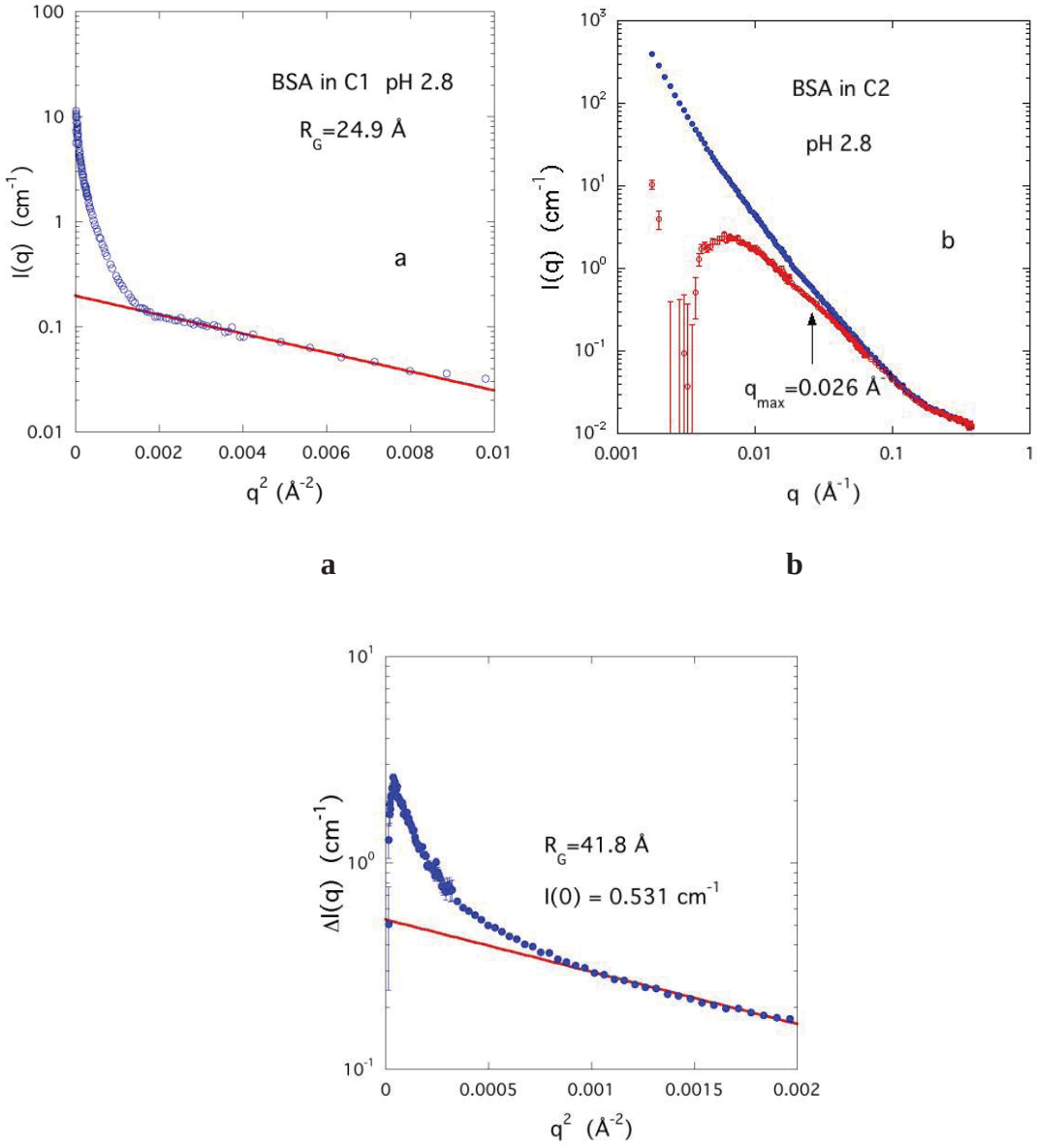

Figure 7. a) Guinier plot of the scattering intensity $I(q)$ of BSA at pH 2.8 in the carbon aerogel C1; the extrapolated intensity of the linear behaviour is $I(0)$=0.197 cm^{-1}. **b)** Total intensity $I(q)$ of BSA at pH 2.8 in carbon C2; lower curve: same data after subtraction of low-q asymptotic power law. **c)** Guinier plot of the data of BSA at pH 2.8 in carbon C2 in the region of the inflection at q_{max}=0.026 Å^{-1} in the difference curve of Figure 7b.

To estimate the mass and aggregation number n of the BSA clusters in the carbon host we employ a model, based on the following assumptions. Protein clusters, each of mass $M_c = nM_W$, are assumed to adsorb on the internal surfaces of the carbon in a random two-dimensional array, with a local order that gives rise to the correlation peak at q_{max} in the scattering pattern. With a triangular array of side $2\pi/q_{max}$ the number of clusters adsorbed on an area S of the sample can thus be evaluated, and hence the concentration of the proteins in the sample that contribute to the correlation peak. Thus

$$c=M_c\, q_{max}^{\,2}\, S\, d_C\, f\, /\, [4\pi^2(\sqrt{3}/2)] \qquad (12)$$

where d_C is the density of the carbon powder and f its filling factor in the sample cell. Elimination of the concentration c from Eqs. 5 and 12 yields for the mass M_c of the clusters

$$M_c=[2\pi N_A/(Kq_{max})]\times[\sqrt{3}\, I(0)/(2S\, f\, d_C)]^{1/2} \qquad (13)$$

Eq. 13 contains six parameters. K is determined for BSA either from Eq. 9 or 10, d_C is listed in Table 1, while S is the incremental mesopore surface area available to particles of diameter $2R$ (**Table 2**). The filling factor f of the carbon particles in the carbon-water slurry is estimated by comparing the intensity of the characteristic scattering peak at 2.0 $Å^{-1}$ from the water in the sample with that in pure D_2O. For C1, the resulting value is f =0.26, while for C2, f=0.35.

Each of the six parameters in the above model is known with a precision of better than 10%. A larger uncertainty, however, is associated with the estimate of the available surface area S (Table 2), which is derived from the adsorption isotherms of nitrogen molecules. [13] For the protein molecules, which are much bulkier than nitrogen, account must be taken of the fact that in the narrowest of the accessible pores, [44] adsorbed proteins are in contact with both walls of the slit. Second and

further layers of proteins can be accommodated only in wider slits, which are less numerous. The effective available surface area may thus be expressed as

$$S_{eff} = S/\sigma \tag{14}$$

where the reduction factor σ ($1 < \sigma < 2$) is a descriptor of the pore size distribution: σ -1 is the fraction of accessible pores that can accommodate no more than one protein layer. Its value is found by comparing M_c calculated from Eq. 13 with the expected mass of the protein clusters, using the appropriate contrast factor (Eq. 9 or 10). Thus, for BSA adsorbed in C1 at pH 6.9, where q_{max}=0.061 Å^{-1} and $I(0)$=0.24 cm^{-1}, the apparent mass of the BSA cluster is

$$M_{c\ app} = 51.5 \text{ kDa} \tag{15}$$

Likewise, for BSA adsorbed in C1 at pH 2.8, where q_{max}=0.056 Å^{-1}and $I(0)$=0.197 cm^{-1} the apparent mass of the BSA cluster is

$$M_{c\ app} = 56.1 \text{ kDa} \tag{16}$$

The evidence from the radius of gyration indicates that in both cases the aggregation number is 1 (i.e., M_c = 66.1 kDa). For consistency with this condition, the surface reduction factor must take the value

$$\sigma = 1.5 \pm 0.1 \tag{17}$$

In other words, in about one half (σ-1=0.5) of the incremental surface area the adsorbed BSA molecules are either in contact with both walls or, by occupying just one wall, prevent a second layer from forming. Although this model is simplistic, the physically plausible value found for σ suggests that it captures the basic features of the correlation peak. The consistency of these findings is evidence that the mass and the radius of gyration of the adsorbed BSA aggregates in C1 are those of a single BSA molecule, both at pH 2.8 and at pH 6.9. The aggregation number of the BSA clusters in C1 is therefore n = 1. The finding that the radius of gyration of BSA in C1

is independent of pH is striking. It suggests that the induced polyelectrolyte character of BSA, which causes it to expand in solution, disappears when the molecule is adsorbed in the carbon pores. In view of the basic nature of this carbon, it seems probable that the excess protons, which in free solution accrete to the basic groups, migrate to the pore walls.

For BSA in carbon C2 at pH 6.9, the value of M_c found in the same way (still assuming $\sigma = 1.5$) is 1.16 MDa, i.e., 17 times the mass of the BSA monomer. These results are listed in **Table 4**. In C2 the situation is thus different from in C1. At pH 6.9, BSA forms large clusters, rather than adsorbing as a monomer. At pH 2.8, by contrast, the correlation peak in the SANS response (**Figure 7b**) is not immediately apparent, being masked by the strong scattering signal at low q from the C2 carbon matrix. Subtraction of the low q asymptotic behaviour (lower curve, Figure 7b) reveals a shoulder at q_{max}~0.026 Å^{-1}, in addition to a broad distribution of diffuse low density clusters. The Guinier plot of the poorly resolved shoulder (**Figure 7c**) is open to greater error, but in this case both the cluster mass M_c =120 kDa, and the radius of gyration R_G = 41.8 Å are consistent with BSA dimers, i.e., the aggregation number is n=2 (Table 4). For consistency, all values of M_c of the adsorbed proteins in Table 4 are calculated taking $\sigma = 1.5$.

The radius of gyration of the BSA molecules adsorbed in the pores of C1 suggests that they are slightly compressed with respect to their size in free solution. In C2, where the BSA clusters contain about 17 monomers, the density of packing $3M_c/(4\pi R^3)$ (assuming solid spheres with $R=(5/3)^{1/2}R_G$) is only slightly lower than that inside the free monomer in solution. This suggests that the monomer-monomer interaction is weakly repulsive. These findings yield the following estimate for the fractal dimension d_f of the clusters,

d_f=log(mass ratio)/log(size ratio) =log(19)/log(99.4/35.6)≈2.87. (18)

This value is consistent with the slope $-d_f$ of the scattering curves in the high q region of Figures 1 and 2. Such a steep slope of the scattering function of BSA reflects the relatively dense internal structure of the BSA molecule.

Table 4

Characteristics of BSA and BPTI aggregates from SANS results

Condition with D_2O	q_{max}	$I(0)$	M_c	R_G	n [(a)]
	$Å^{-1}$	cm^{-1}	kDa	Å	
BSA solution pH 6.9 (10 g/L)	0.031	0.885	66.1[(b)]	27.6	1
BSA solution pH 2.8	0.027	0.685	66.1[(b)]	38.9	1
BSA in C1 pH 6.9	0.061	0.24	63.1[(c)]	24.9	1
BSA in C2 pH 6.9	0.048	5.0	1250[(c)]	77	17
BSA in C1 pH 2.8	0.056	0.197	68.7[(c)]	24.9	1
BSA in C2 pH 2.8	0.026	0.531	120±15[(c)]	41.8	2
BPTI solution	-	0.0417	6.51[(b)]	9.8	1
BPTI in C1 pH 6.9	0.048	0.149	73.2[(c)]	23.5	11
BPTI in C2 pH 6.9	0.0071	2.03	1170[(c)]	122	175

[(a)] aggregation number, n; [(b)] $M_c = M_W$, [(c)] $\sigma = 1.5$

3.2.2. BPTI

Measurements of the BPTI molecules adsorbed in the carbons were made only

at pH 6.9. The SANS response of BPTI in C1 is shown in the Guinier representation in **Figure 8a**. With the correlation peak q_{max}=0.048 Å^{-1} and the extrapolated intensity $I(0)$=0.149 cm^{-1}, Eq. 13 yields for this system (still assuming σ=1.5)

$$M_c = 73.2 \text{ kDa} \tag{19}$$

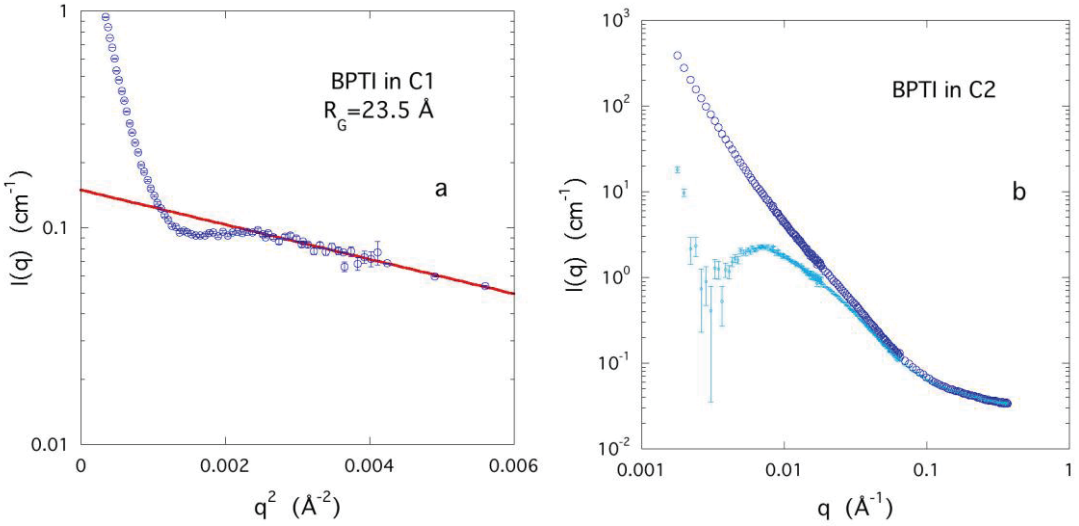

Figure 8. a) Guinier plot of the scattering intensity $I(q)$ of BPTI in the carbon aerogel C1; the extrapolated intensity of the linear behaviour is $I(0)$=0.149 cm^{-1}, with R_G=23.5Å; **b)** Total intensity $I(q)$ of BPTI in carbon C2; lower curve: same data after subtraction of low q asymptote.

The above estimated value of M_c assumes that the contrast factor K^2 for BPTI in the carbon remains the same as in free solution (Eq. 11). The apparent fractal dimension of the BPTI clusters, calculated according to Eq. 19, is

$$d_f \approx 2.5 \tag{20}$$

This packing, which is more open than that of BSA, is consistent with a branched like arrangement of the BPTI monomers.

For BPTI in C2, as with BSA in C2, the total scattering curve (**Figure 8b**) displays no clearly resolved correlation peak. At low q the response exhibits power law behaviour with a slope of approximately -2.9. Subtraction of the power law yields

the lower curve in Figure 8b, with a maximum at q_{max}=0.00708 Å^{-1}. In a Guinier representation similar to Figure 8a (not shown) these data yield $I(0)$=2.93 cm^{-1}, with R_G=122 Å, which corresponds to an aggregation number n=175. The internal concentration of these clusters is much smaller than those in C1. They are the counterpart of the similar broad peak noted above at q≈0.0065 Å^{-1} in Figure 7b.

3.3. Protein concentration distribution

The above model counts only those protein molecules that contribute to the correlation peak in the SANS response. However, clusters of proteins occupying pores that are too large to be detected by the measurements, and molecules that do not possess the local order assumed in the model, also contribute to the total concentration. The concentration c defined in Eq. 12 is therefore not the total concentration of protein adsorbed in the carbons. The total concentration must be estimated from the whole scattering curve.

The overall protein distribution can be found by using the q-dependent intensity ratios $u_1(q)=I_{C\_D2O}(q)/I_C(q)$ and $u_2(q)=I_{C\_protein\_D2O}(q)/I_C(q)$ to derive the concentration distribution $c(q)$ of the proteins in reciprocal space (see Supplementary Information). In these ratios the numerators are respectively the signal from a carbon sample containing D_2O and the same carbon sample with the protein solution, while the denominator is that of the dry carbon. For BSA at pH 6.9, the result (**Figure 9**) shows, firstly, that segments larger than about $2\pi/0.31$≈20 Å do not penetrate into either carbon, and, secondly, that in C2 the smaller pores (higher q range) are substantially less populated than those in C1.

Closely similar results are found for pH 2.8. The mean concentration of BSA inside the carbon samples (in g/mL) can then be found from the second moment of

this concentration distribution

$$< c >= \int_0^{qmax} c(q)q^2\, dq / \int_0^{qmax} q^2 dq \qquad (21)$$

where q_{max} = 0.31 Å^{-1} is the point of cut-off in Figure 9 imposed by steric exclusion. Finally, multiplication by the available volume V in each sample (Table 2) yields the total BSA content in the carbons. Thus

for C1, $<c>V$ = 0.40 g/g

and for C2, $<c>V$ = 0.14 g/g.

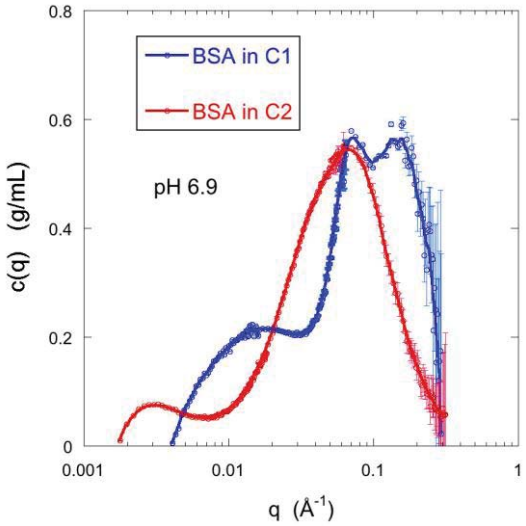

Figure 9. Concentration distribution $c(q)$ of BSA in the C1 and C2 carbon particles (see Supplementary Information). The cut-off at high q occurs in both samples at q ≈0.31 Å^{-1}. The trend $c(q)\rightarrow 0$ at q<0.01 Å^{-1} in C1 is an artefact from the excess surface scattering of C1 in pure D_2O. Continuous lines are guides for the eye.

Table 5 compares the above findings with the direct measurements of protein adsorption from reference [13]. The total amount of protein adsorbed by the carbons found from SANS is in semi-quantitative agreement with the direct findings. In these estimates, however, it should be recalled, firstly, that precise equality of the filling factors of the corresponding dry and wet carbons is difficult to achieve, and secondly,

the region close to the cut-off point q_{max}, which contributes the most to the second moment (Eq. 21), is the region of greatest uncertainty in $c(q)$. Nevertheless, the concentration distributions $c(q)$ obtained by this method offer an indicator of the real distribution of the proteins in the sample.

Table 5. Protein adsorption capacity of carbons C1 and C2

Sample	adsorbed BSA (direct measurement)	adsorbed BSA (SANS)	adsorbed BPTI (direct measurement)	adsorbed BPTI (SANS)
	g/g			
C1 in water pH 6.9 (unbuffered)	0.42	0.38	1.1	0.60
C2 in water pH 6.9 (unbuffered)	0.09	0.16	0.27	0.16
C1 pH 3	0.28	0.42	-	
C2 pH 3	0.07	0.08	-	

Although the nitrogen adsorption measurements of ref. [13] show that in both of the dry carbons C1 and C2 the pore sizes are sufficient to accommodate single BSA molecules, the present observations indicate that the hydrophobic carbon C1 absorbs BSA more readily than the hydrophilic C2. The latter result appears at first sight to contradict observations according to which BSA becomes less mobile and more strongly attached to hydrophilic surfaces than to hydrophobic surfaces [6, 45]. Strong adhesion, however, hinders the diffusion of proteins in small pores: when the

BSA solution enters the hydrophilic C2 carbon, the proteins penetrate no farther than the pore entrance, where they are immediately immobilised, blocking access to other molecules. In C1, by contrast, where adhesive forces are weaker because of the absence of polar groups, the proteins diffuse more freely inside the pores and occupy the available surface area. The difference in hydrophilic character between C1 and C2 is sufficient to explain their different adsorption capacities.

4. Conclusions

BSA is adsorbed by both the carbon aerogels C1 and C2, the former of which has a higher mesopore content. In spite of its larger BET surface area, the adsorption capacity of C2 for both BSA and BPTI is only about a quarter of that of C1. The SANS observations indicate that clusters of proteins may form in the pores. In C1, the aggregation number for BSA is n=1, i.e., the protein is adsorbed in the form of monomers, with a slightly compressed radius of gyration. In the same carbon at pH 2.8, the extended conformation adopted in free solution by BSA at low pH does not occur: in the basic environment of carbon C1 the indirect polyelectrolyte character of this molecule induced by the pH disappears as the excess proton amount is transferred to the pore walls. In C2 the aggregation number for BSA is larger, about 17, confirming the aggregated state of the protein. For the smaller BPTI molecule, the aggregation number is of the order of 10 in C1, and more than an order of magnitude greater in C2. The model employed to obtain these results is based on the incremental surface area S of the carbon deduced from the nitrogen adsorption measurements. Owing to the size of the proteins, this surface area is further diminished by a factor σ, where σ-1 is the fraction of pores of width that accommodate no more than one layer of protein molecules. The finding here that σ~1.5 in the carbon C1 implies that in

about 50% of the incremental surface the proteins are in contact with both walls.

In the hydrophilic carbon sample C2, both proteins form aggregates. The comparison of these two carbons implies that the greater adsorption capacity of C1 is in part attributable to its wider pores, but also to weak adhesion of the proteins to the hydrophobic surfaces, which allows them to migrate inside the pores. In C2, by contrast, the proteins are immobilised by their strong attraction to the hydrophilic surface, thus blocking access to and preventing penetration into the smaller pores. This finding illustrates the important role of surface chemistry in the adsorption of proteins in porous substrates.

Acknowledgements

We are grateful to the Institut Laue-Langevin, Grenoble, France for access to the D11 and D16 instruments and also to the European Synchrotron Radiation Facility for access to the French CRG beam line BM02. Financial support from the Marie Curie International Research Staff Exchange Scheme (ENSOR, Grant No. 269267), the Marie Curie Reintegration grant, PERG08-GA-2010-276954, and OTKA K109558 is acknowledged. AT recognizes the support of TÁMOP 4.2.4. A/1-11-1-2012-0001 "National Excellence Program – Elaborating and operating an inland student and researcher personal support system". The project was subsidized by the European Union and co-financed by the European Social Fund.

References

[1] Riccardi E, Wang JC, Liapis AI. Protein adsorption in porous adsorbent particles: a multiscale modeling study on inner radial humps in the concentration profiles of adsorbed protein induced by nonuniform ligand density distributions. J Sep Sci. 2009; 32(18):3084-98

[2] Ge S, Kojio K, Takahara A, Kajiyama T. Bovine serum albumin adsorption onto immobilized organotrichlorosilane surface: influence of the phase separation on

protein adsorption patterns. Journal of Biomaterials Science. Polymer Edition 1998; 9: 131–150.
[3] Bales RC, Hinkle SR, Kroeger TW, Stocking K, Gerba CP. Bacteriophage adsorption during transport through porous media: chemical perturbations and reversibility Environ. Sci. Technol., 1991; 25 (12): 2088–2095
[4] Kisler JM, Stevens GW, O'Connor AJ. Adsorption of proteins on mesoporous molecular sieves. Mater.Phys.Mech. 2001; 4:89-93
[5] Koshari SHS, Wagner NJ, Lenhoff AM. Characterization of lysozyme adsorption in cellulosic chromatographic materials using small-angle neutron scattering, J. Chromatogr. A. 2015; 1399: 45–52.
[6] Jeyachandran YL, Mielczarski E, Rai B, Mielczarski JA. Quantitative and Qualitative Evaluation of Adsorption/Desorption of Bovine Serum Albumin on Hydrophilic and Hydrophobic Surfaces Langmuir 2009; 25(19): 11614–11620.
[7] Lazzara TD, Mey I, Steinem C, Janshoff A. Benefits and Limitations of Porous Substrates as Biosensors for Protein Adsorption Anal.Chem. 2011; 83: 5624-5630
[8] Sandeman S, Petersson M, Wiezell S, Howell C, Phillips G, Zheng Y, Tennison S, Kozynchenko O, Mikhalovsky S Characterising Nanoporous Carbon Adsorbents for Biological Application to Chronic Kidney Disease. Journal of Biomaterials and Tissue Engineering 2012; 2: 40–47.
[9] Howell CA, Sandeman SR, Phillips GJ, Mikhalovsky SV, Tennison SR, Rawlinson AP, Kozynchenko OP. Nanoporous activated carbon beads and monolithic columns as effective hemoadsorbents for inflammatory cytokines. Int. J. Artif. Organs 2013; 36: 624-32.
[10] László K, Czakkel O, Dobos G, Lodewyckx P, Rochas C, Geissler E. Water vapour adsorption in highly porous carbons as seen by small and wide angle X-ray scattering. Carbon 2010; 48; 1038 –48.
[11] Radlinski AP, Mastalerz M, Hinde AL, et al., Application of SAXS and SANS in evaluation of porosity, pore size distribution and surface area of coal. International Journal of Coal Geology 2004; 59: 245 – 271
[12] László K, Czakkel O, Demé B, Geissler E. Simultaneous adsorption of toluene and water vapor on a high surface area carbon. Carbon 2012; 50: 4155 – 62.
[13] Nagy B, Tóth A, Savina I, Mikhalovsky S, Mikhalovska L, Geissler E, László K. Adsorption of Globular Proteins by High Surface Area Porous Carbons (in

preparation)
[14] Tennison RS. Phenolic-resin-derived activated carbons. Applied Catalysis A 1998; 173: 289-311.
[15] Gun'ko VM, Meikle ST, Kozynchenko OP, Tennison SR, Ehrburger-Dolle F, Morfin I, Mikhalovsky SV. Comparative Characterization of Carbon Adsorbents and Polymer Precursors by Small-Angle X-ray Scattering and Nitrogen Adsorption Methods J. Phys. Chem. C 2011; 115: 10727–10735.
[16] Gun'ko VM, Turov VV, Kozynchenko OP, Nikolaev VG, Tennison SR, Meikle ST, Snezhkova EA, Sidorenko AS, Ehrburger-Dolle F, Morfin I, Klymchuk DO, Mikhalovsky SV Activation and structural and adsorption features of activated carbons with highly developed micro-, meso- and macroporosity Adsorption 2011; 17: 453–460.
[17] Gun'ko VM, Turov VV, Kozynchenko OP, Nikolaev VG, Tennison SR, Meikle ST, Snezhkova EA, Sidorenko AS, Ehrburger-Dolle F, Morfin I, Klymchuk DO, Mikhalovsky SV. Activation and structural and adsorption features of activated carbons with highly developed micro-, meso- and macroporosity Adsorption 2011; 17: 453–460.
[18] Budayova-Spano M, Lafont S, Astier J-P, Ebel C, Veesler S. Comparison of solubility and interactions of aprotinin (BPTI) solutions in H_2O and D_2O. Journal of Crystal Growth 2000; 217; 311–319.
[19] Glasoe PK, Long FA. Use of glass electrodes to measure acidities in deuterium oxide J. Phys. Chem. 1960; 64: 188–190.
[20] Brunauer S, Emmett P, Teller E. Adsorption of gases in multimolecular layers. J. Am. Chem. Soc. 1938; 60: 309–319.
[21] Dubinin MM, Radushkevich LV. Equation of the Characteristic Curve of Activated. Charcoal. Proc. Acad. Sci. USSR Phys. Chem. Sect. 1947; 55: 331–337.
[22] Landers J, Gor GY, Neimark AV. Density functional theory methods for characterization of porous materials. Colloids Surfaces A Physicochem. Eng. Asp. 2013; 437: 3–32.
[23] Horkay F, Hecht A-M, Mallam S, Geissler E, Rennie AR. Microscopic and macroscopic thermodynamic observations in swollen poly(dimethyl siloxane) networks. Macromolecules 1991; 24: 2896-2902.
[24] El Kadi N, Taulier N, Le Huérou JY, Gindre M, Urbach W, Nwigwe I, Kahn PC, Waks M. Unfolding and Refolding of Bovine Serum Albumin at Acid pH: Ultrasound

and Structural Studies. Biophys J. 2006; 91: 3397–3404.
[25] Sadler PJ, Tucker A. pH-induced structural transitions of bovine serum albumin Histidine pK, values and unfolding of the N-terminus during the N to F transition. Eur. J. Biochem. 1993; 212: 811-817.
[26] Nierlich M, Williams CE, Boué F, Cotton JP, Daoud M, Farnoux B, Jannink G, Picot C, Moan M, Wol C, Rinaudo M, de Gennes PG. Small angle neutron scattering by semi-dilute solutions of polyelectrolyte. J. Physique (Paris) 1979; 40: 701-704.
[27] Hayter JB, Penfold J. An analytic structure factor for macroion solutions, Molecular Physics 1981; 42:109-118.
[28] Kotlarchyk M, Chen SH. Analysis of small angle neutron scattering spectra from polydisperse interacting colloids. J. Chem. Phys. 1983; 79: 2461-2469.
[29] Squire PG, Moser P, O'Konsky CT. Hydrodynamic properties of bovine serum albumin monomer and dimer. Biochemistry 1968; 7: 4261-4272.
[30] Nossal R, Glinka CJ, Chen SH. SANS Studies of Concentrated Protein Solutions. I. Bovine Serum Albumin Biopolymers 1986; 25: 1157-1175.
[31] Bendedouch D, Chen SH. Structure and Interparticle Interactions of bovine serum albumin in solution studied by small-Angle neutron scattering J. Phys. Chem. l983; 87: 1473-1477.
[32] Wright AK, Thompson MR. Hydrodynamic structure of bovine serum albumin determined by transient electric birefringence. Biophys. J. 1975; 15 (2 Pt 1): 137–141
[33] Serdyuk IN, Zaccai NR, Zaccai J. Methods in Molecular Biophysics: Structure, Dynamics, Function, Cambridge University Press, 2007. ISBN: 9780511276118
[34] Posselt D, Pederson JS, Mortensen K. A SANS investigation on absolute scale of a homologous series of base-catalysed silica aerogels J. Non-Cryst. Solids 1992; 145: 128-132
[35] Carter DC, Ho JX. Structure of Serum Albumin. Adv. Protein Chem. 1994; 45: 153-203.
[36] Santos SF, Zanette D, Fischer H, Itri R. A systematic study of bovine serum albumin (BSA) and sodium dodecyl sulfate (SDS) interactions by surface tension and small angle X-ray scattering. J. Coll. Interf. Sci. 2003; 262: 400-8.
[37] Kamal JKA, Zhao L, Zewail AH. Ultrafast hydration dynamics in protein unfolding: Human serum albumin. Proc. Natl. Acad. Sci. USA 2004; 101: 13411-13416.

[38] Fritz H, Wunderer G. Biochemistry and applications of aprotinin, the kallikrein inhibitor from bovine organs. Arzneim.-Forsch./Drug Res. 1983; 33 (I) Nr. 4: 479-494.
[39] Appavou MS, Gibrat G, Bellissent-Funel MC. Influence of pressure on structure and dynamics of bovine pancreatic trypsin inhibitor (BPTI): Small angle and quasi-elastic neutron scattering studies. Biochimica et Biophysica Acta 2006; 1764: 414-423
[40] Porod G. In: Kratky O, Glatter O, editors. Small Angle X-ray Scattering. London: Academic (1982).
[41] Pfeifer P. Fractal dimension as working tool for surface-roughness problems. Applications of Surface Science 1984; 18: 146-164.
[42] Leon y Leon CA, Radovic LR. Interfacial chemistry and electrochemistry of carbon surfaces. In: Thrower PA, editor. Chemistry and Physics of Carbon, 24; 213-310: Marcel Dekker (1994)
[43] László K, Czakkel O, Josepovits K, Rochas C, Geissler E. Influence of surface chemistry on the SAXS response of polymer-based activated carbons. Langmuir 2005; 21: 8443-8451.
[44] Mascotto S, Kuzmicz D, Wallacher D, Siebenbürger M, Clemens D, Risse S, Yuan J, Antonietti M, Ballauff M. Poly(ionic liquid)-derived nanoporous carbon analyzed by combination of gas physisorption and small-angle neutron scattering Carbon 2015; 82: 425 –435
[45] Rabe M, Verdes D, Seeger S. Surface-induced spreading phenomenon of protein clusters. Soft Matter 2009; 5: 1039–1047.

Figure(s)
Click here to download high resolution image

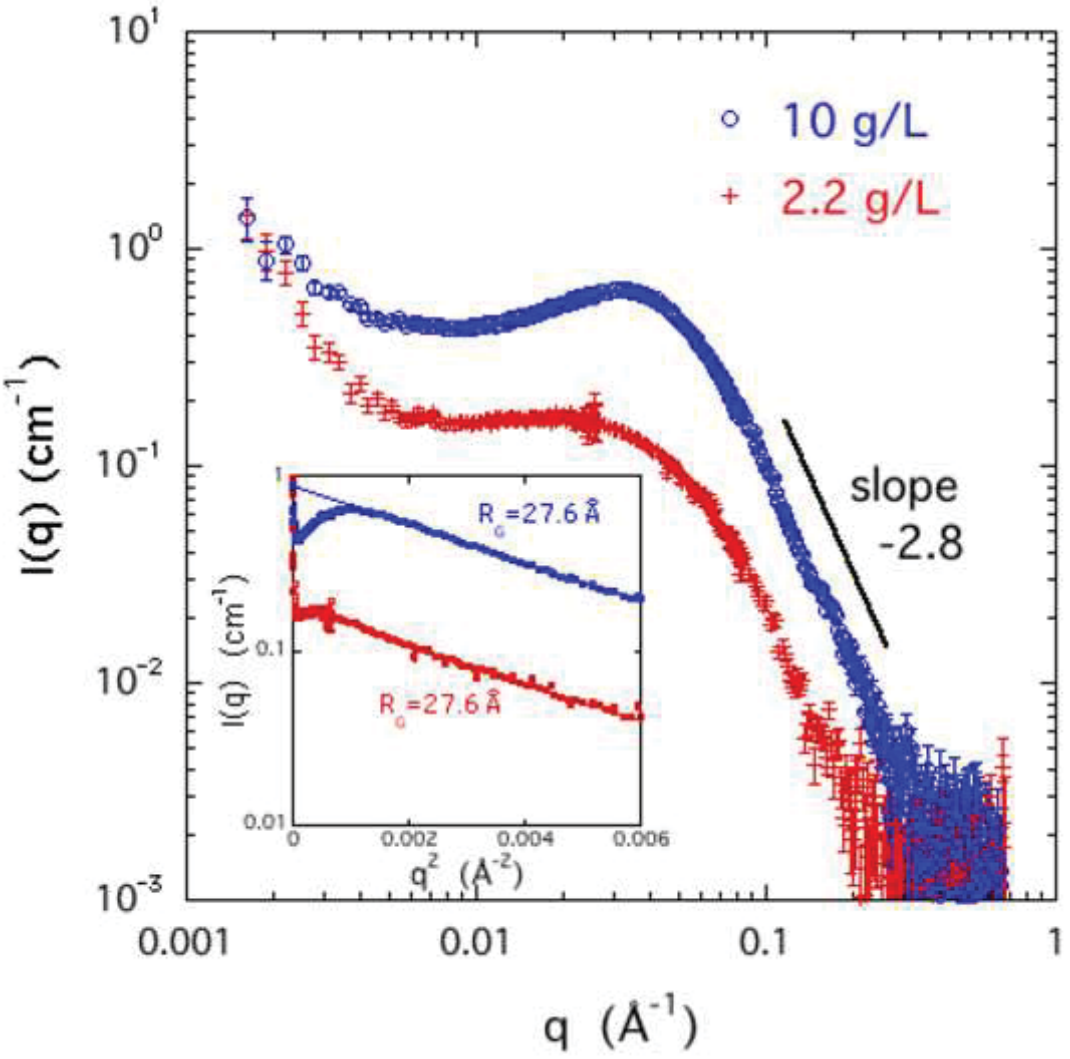

Figure(s)
Click here to download high resolution image

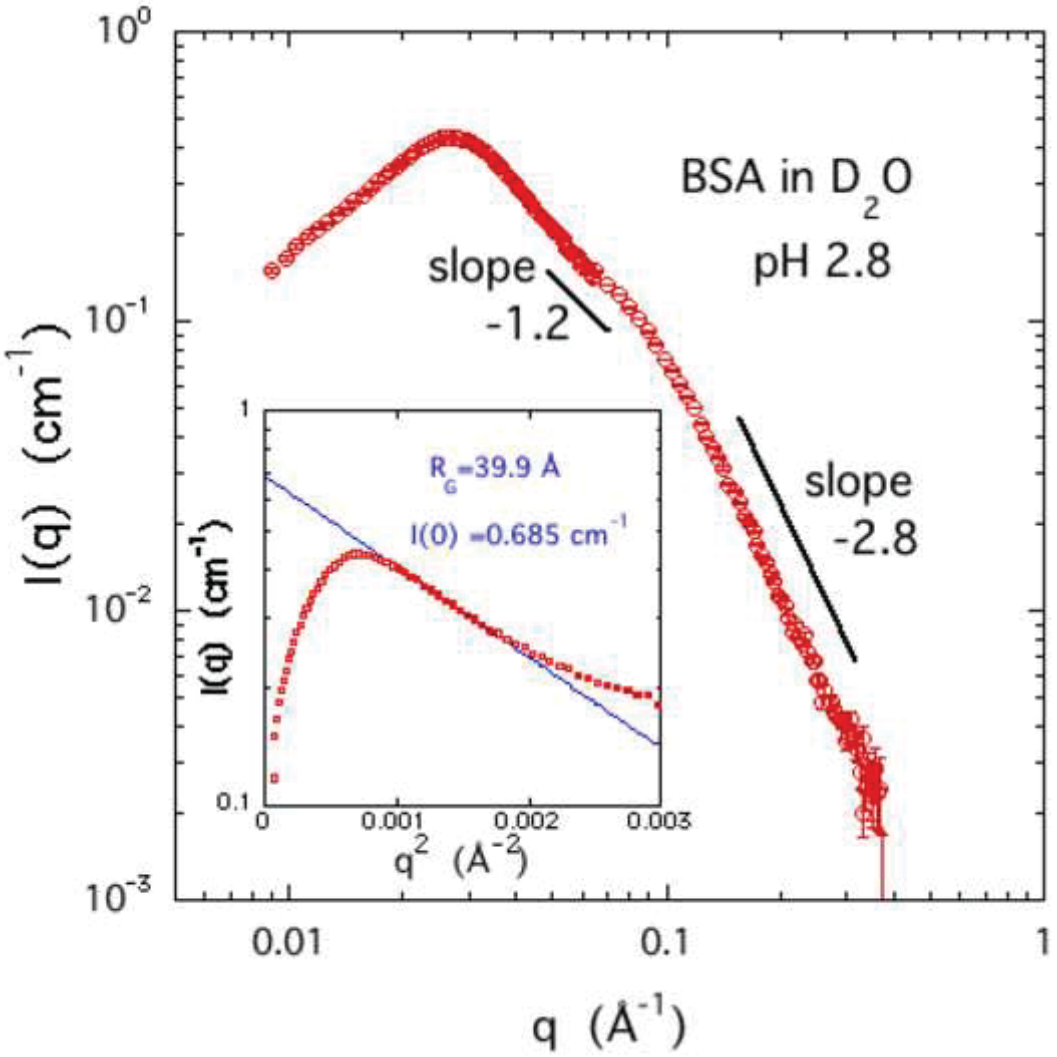

Figure(s)
Click here to download high resolution image

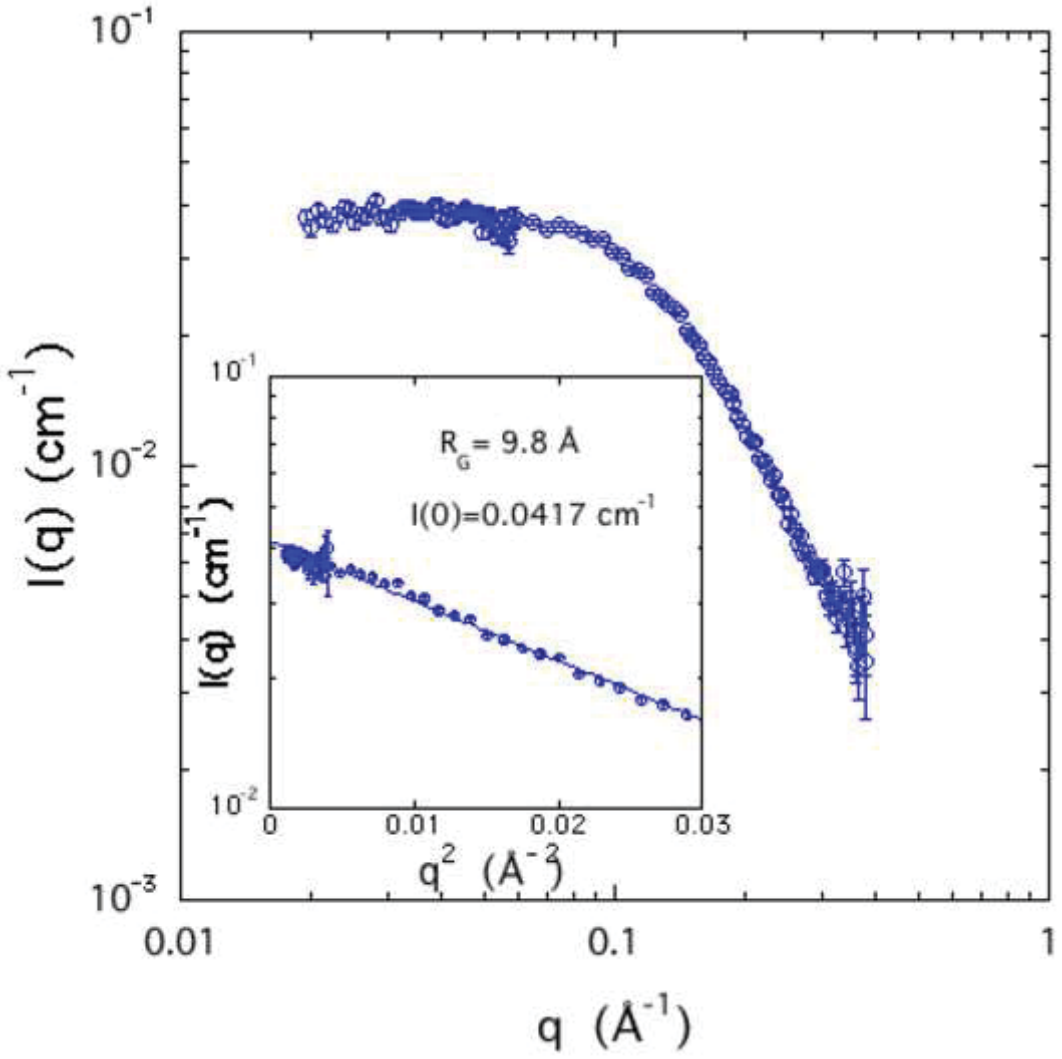

Figure(s)
Click here to download high resolution image

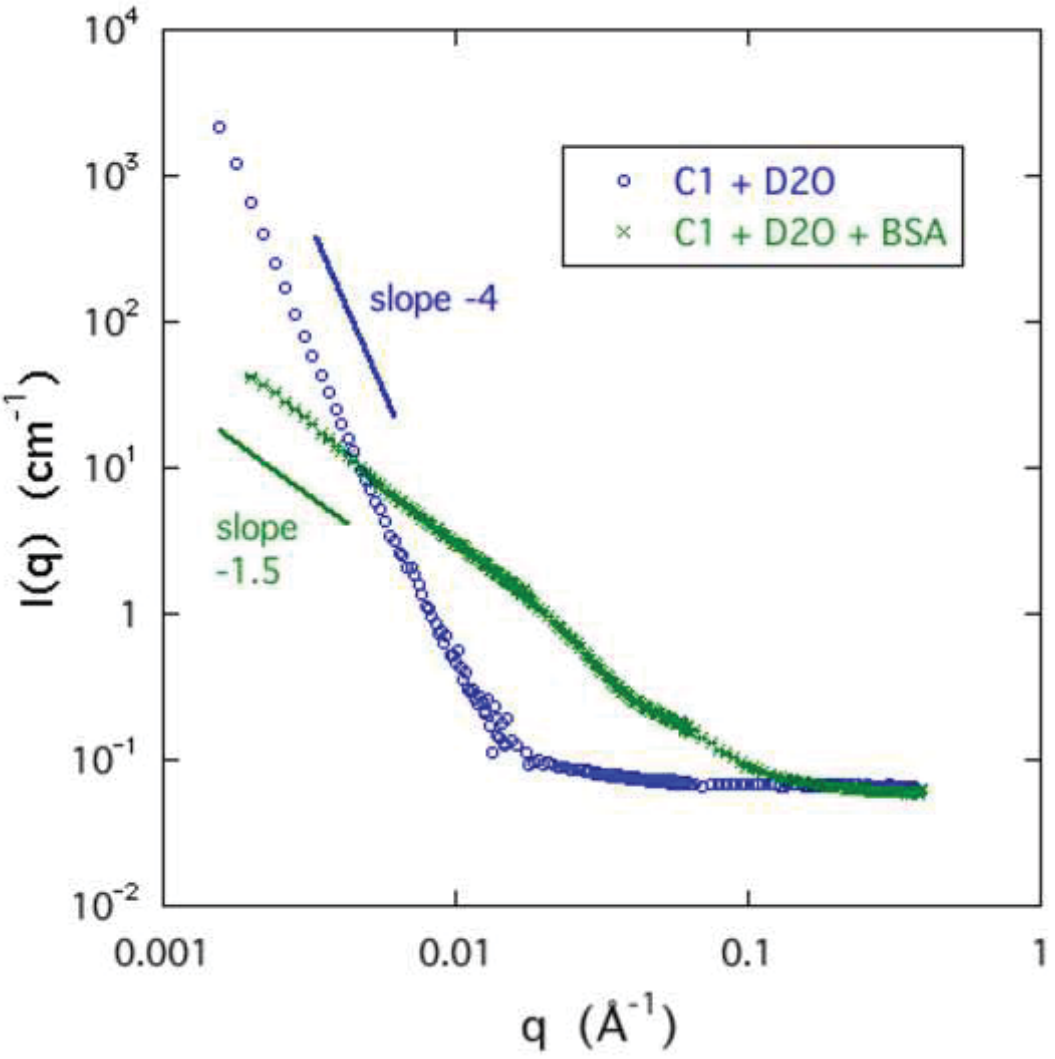

Figure(s)
Click here to download high resolution image

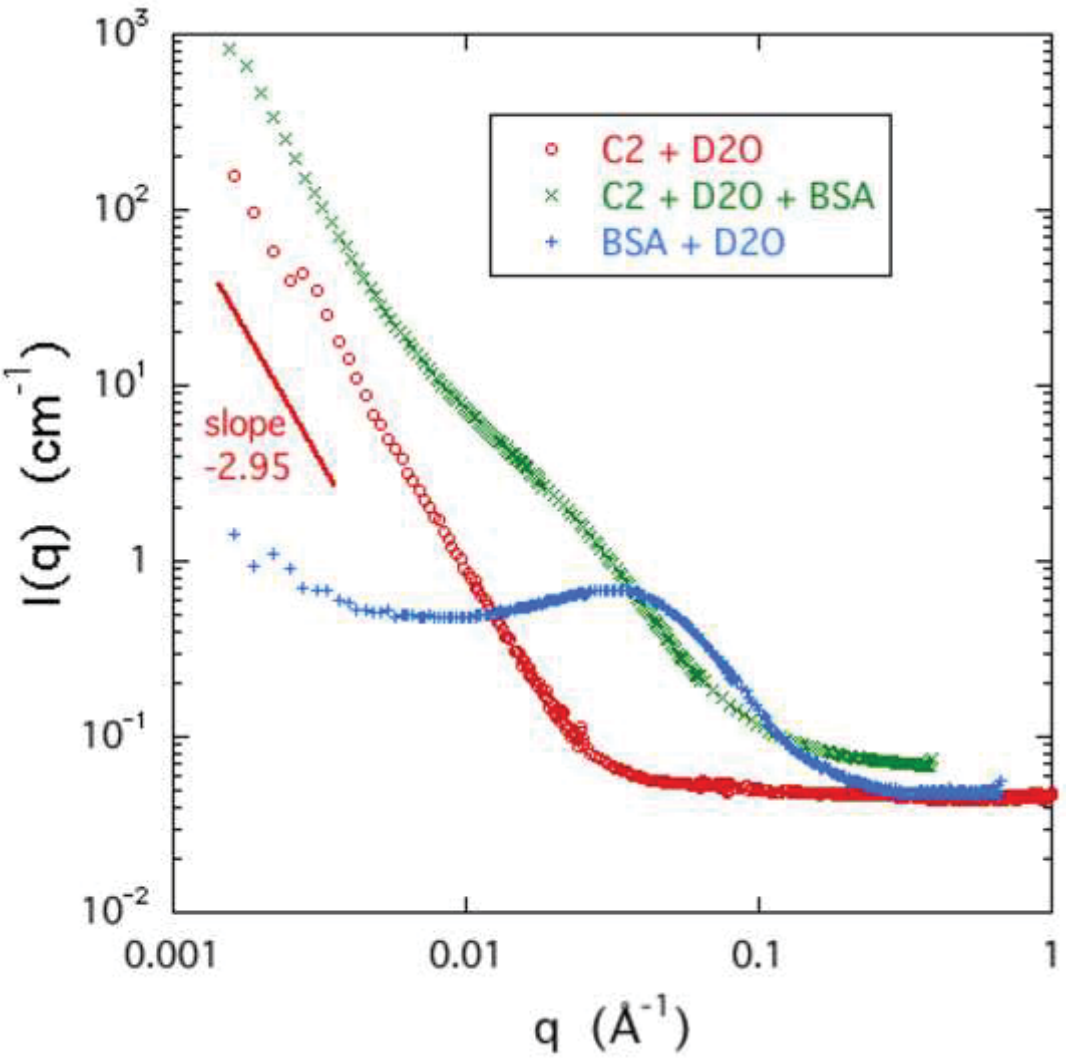

Figure(s)
Click here to download high resolution image

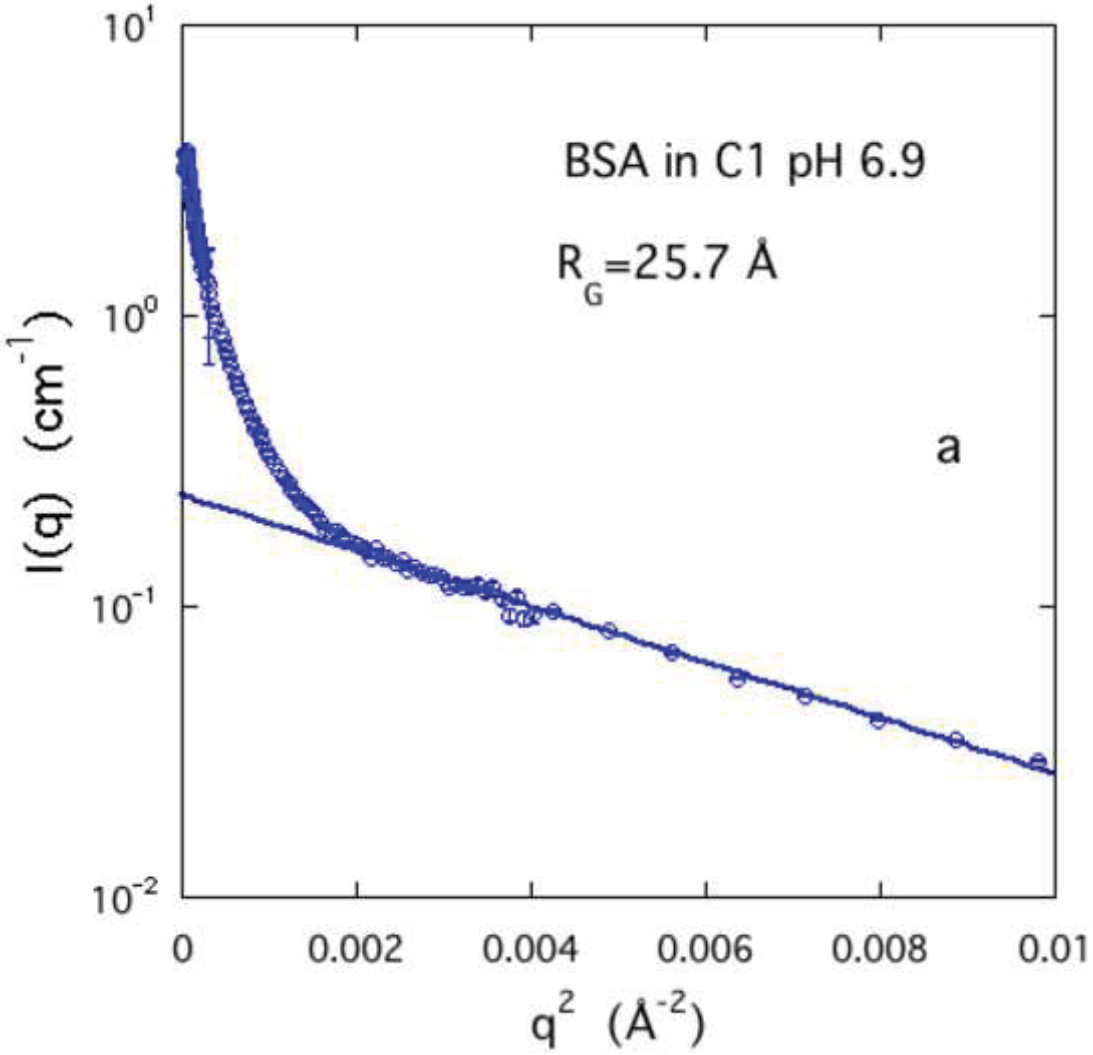

Figure(s)
Click here to download high resolution image

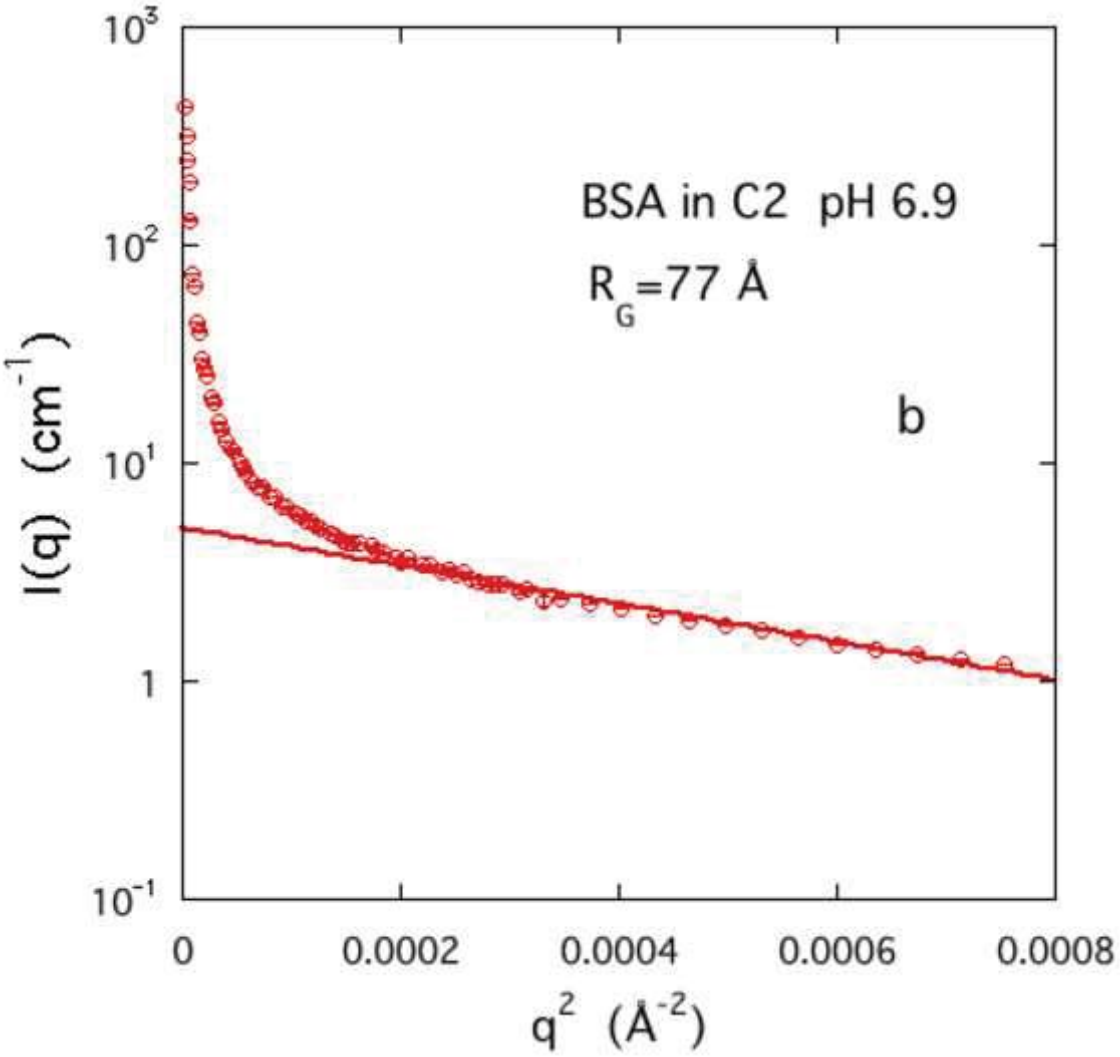

Figure(s)
Click here to download high resolution image

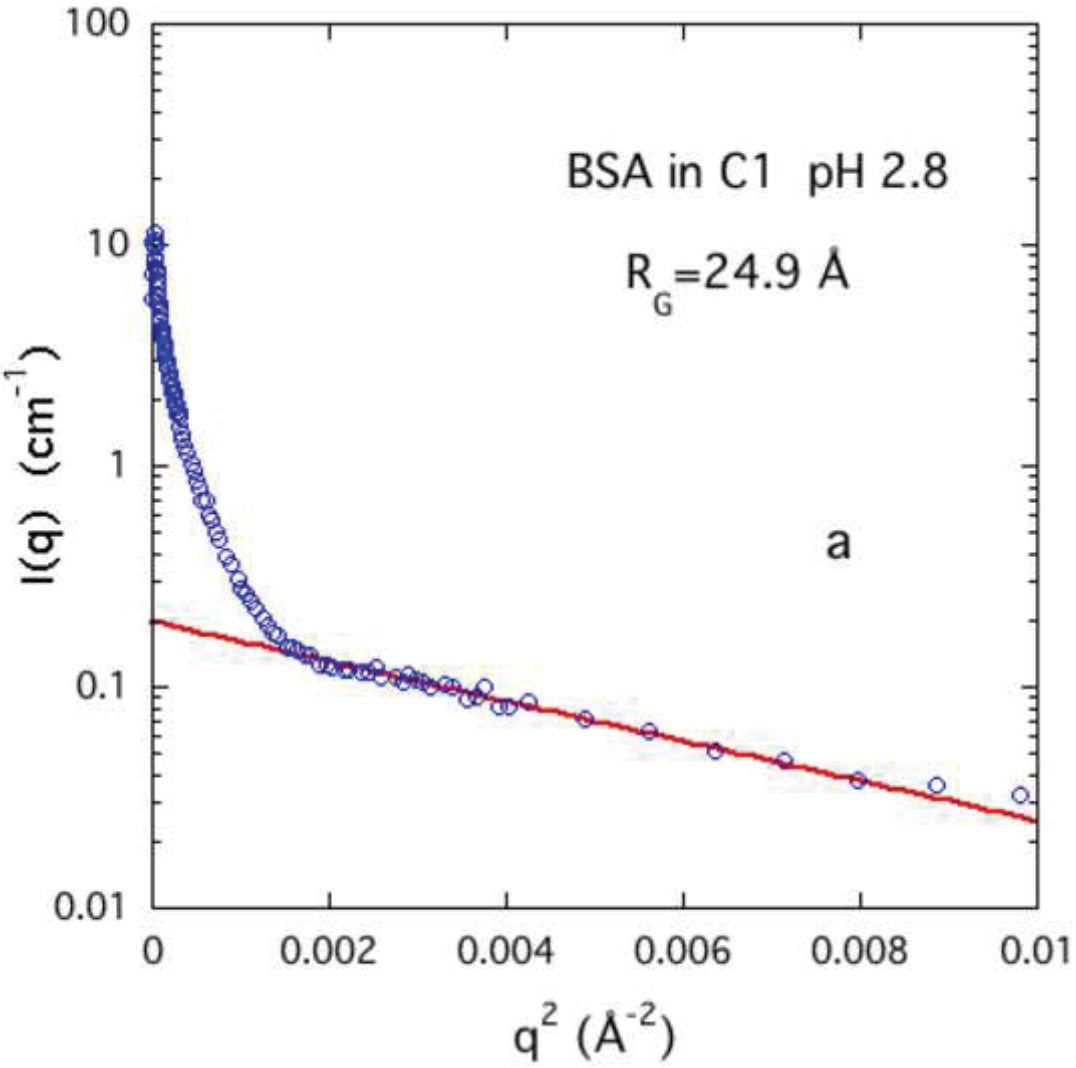

Figure(s)
Click here to download high resolution image

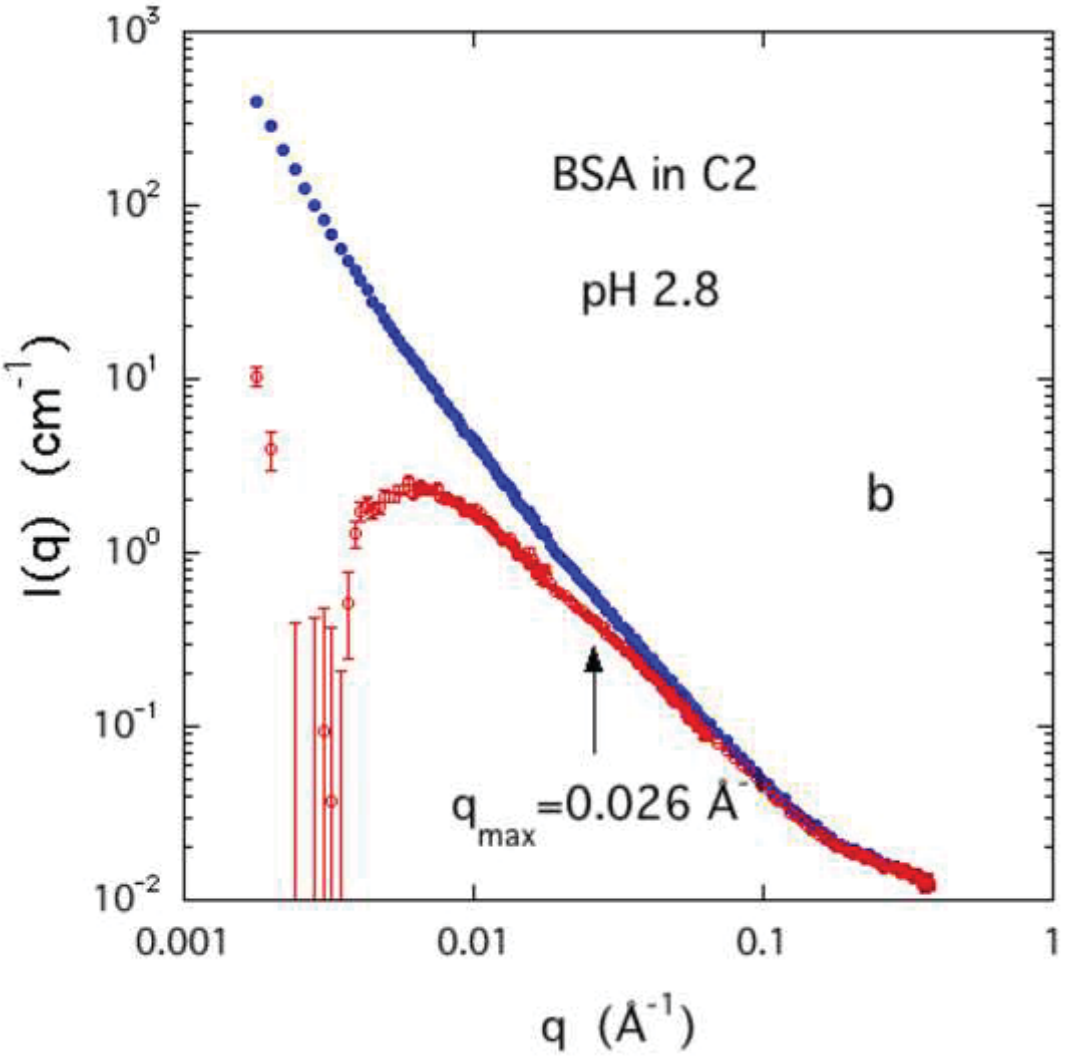

Figure(s)
Click here to download high resolution image

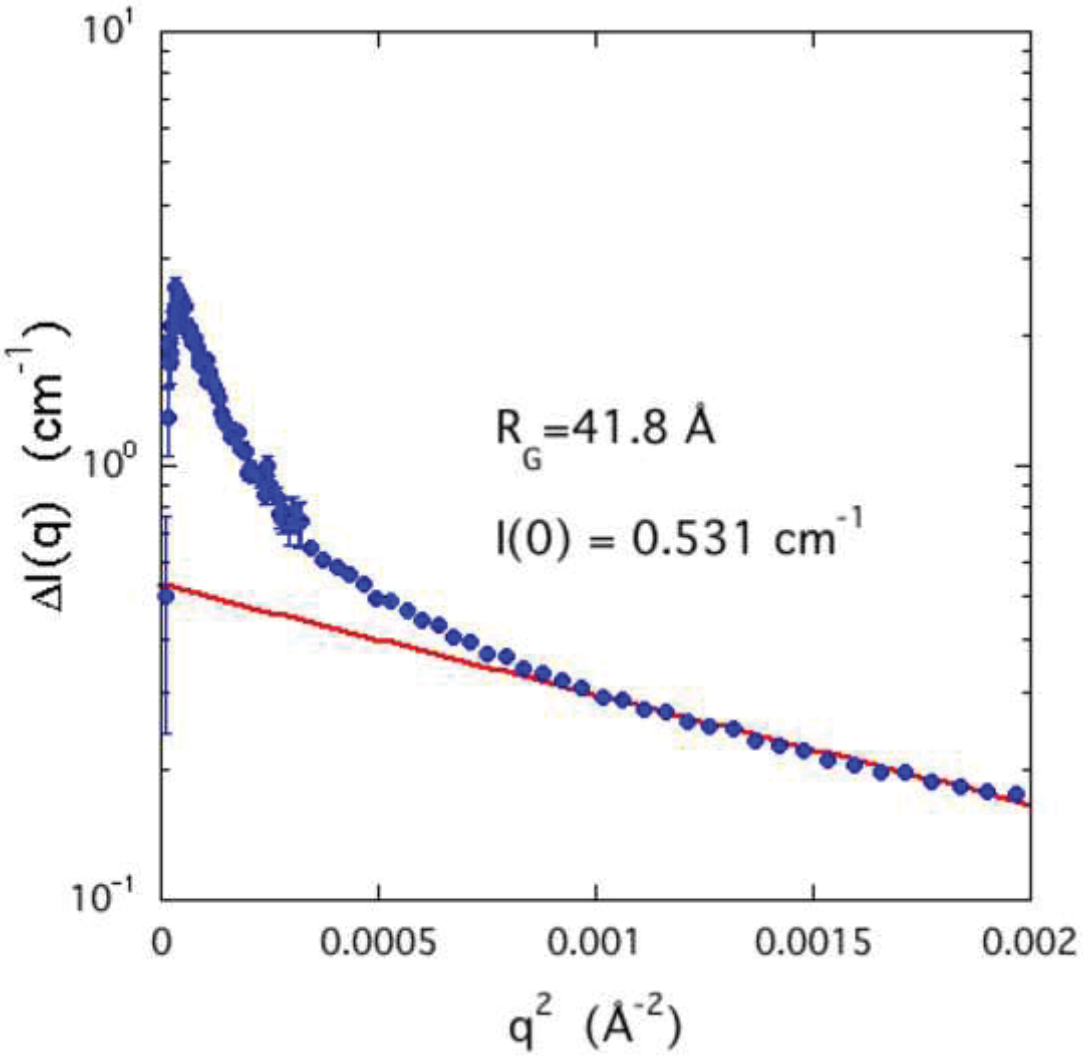

Figure(s)
Click here to download high resolution image

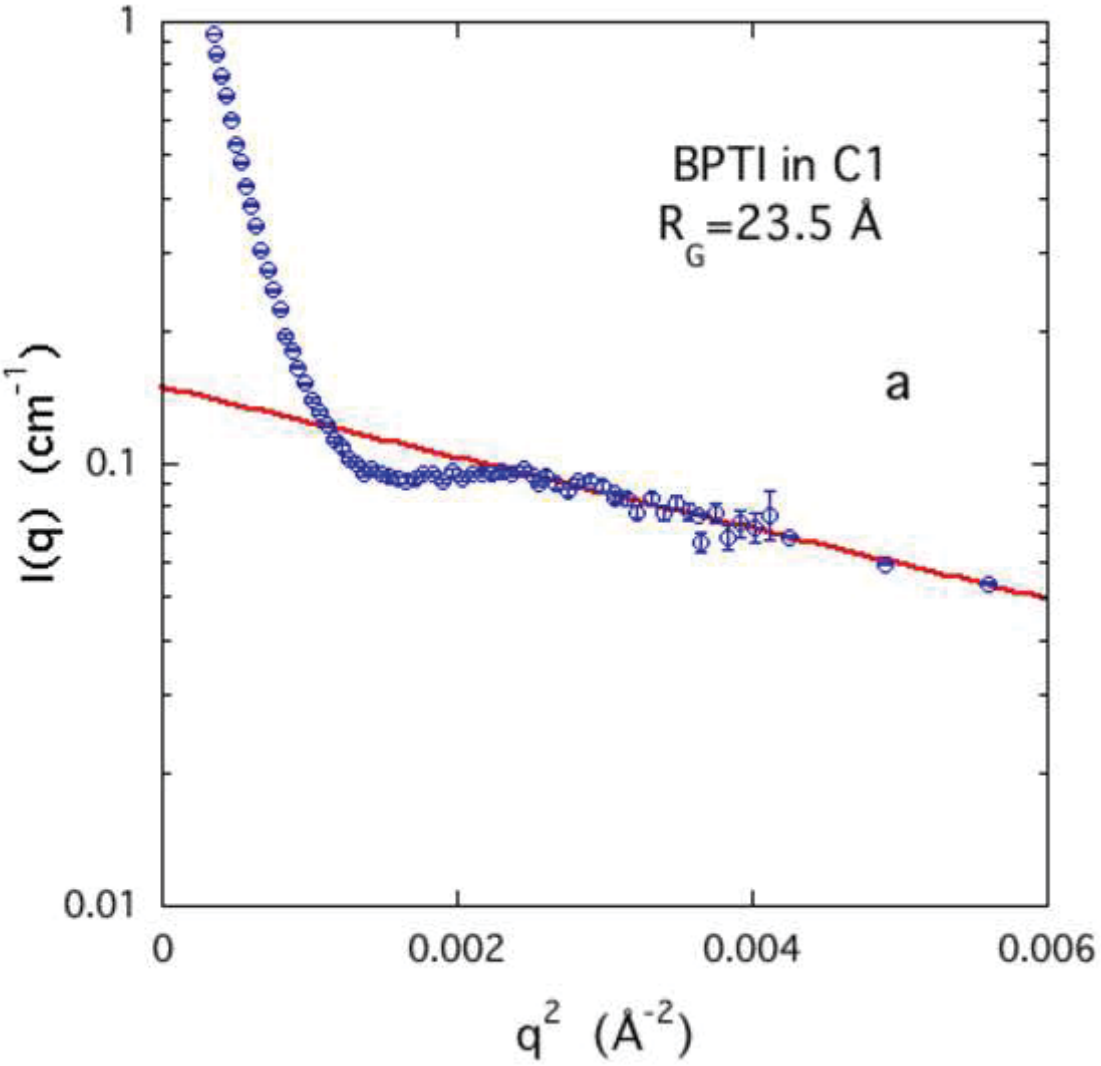

Figure(s)
Click here to download high resolution image

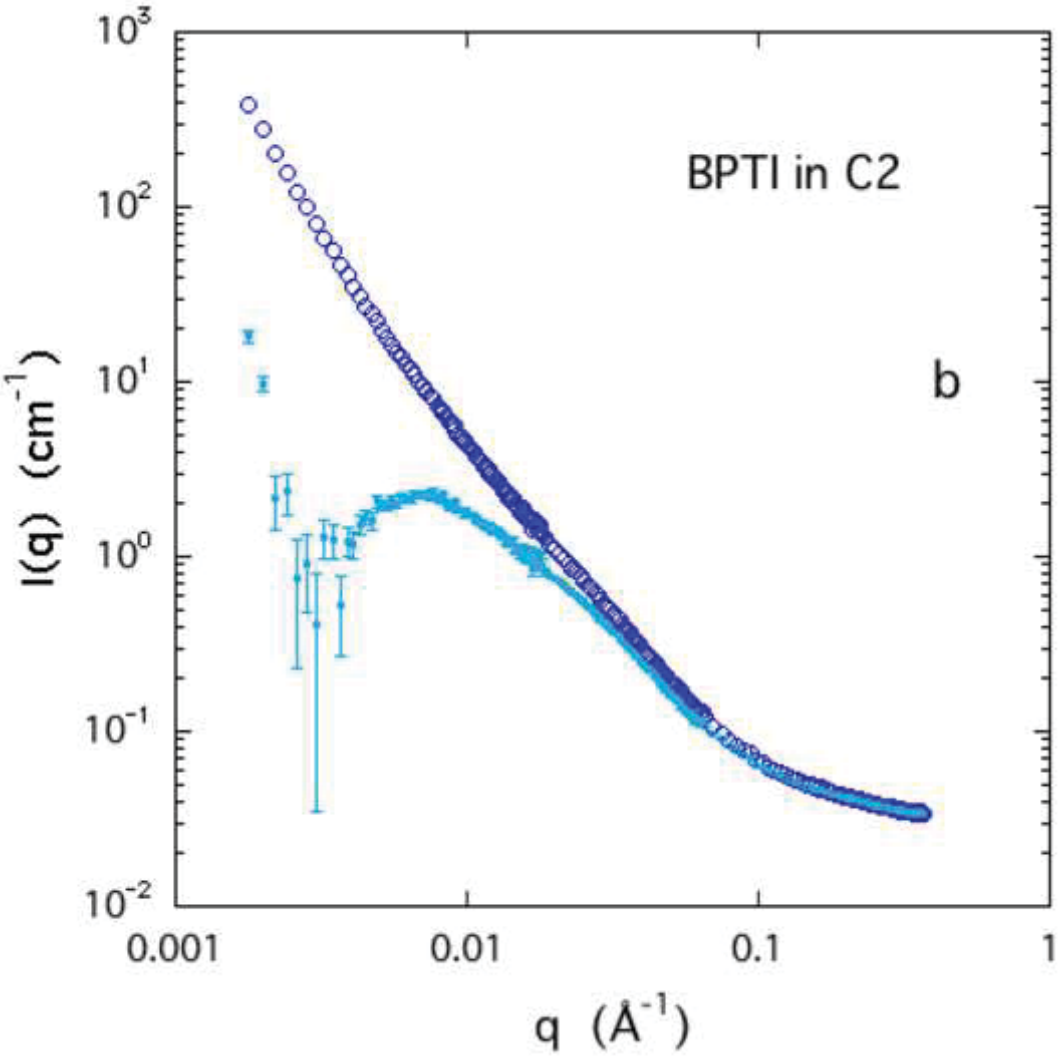

Figure(s)
Click here to download high resolution image

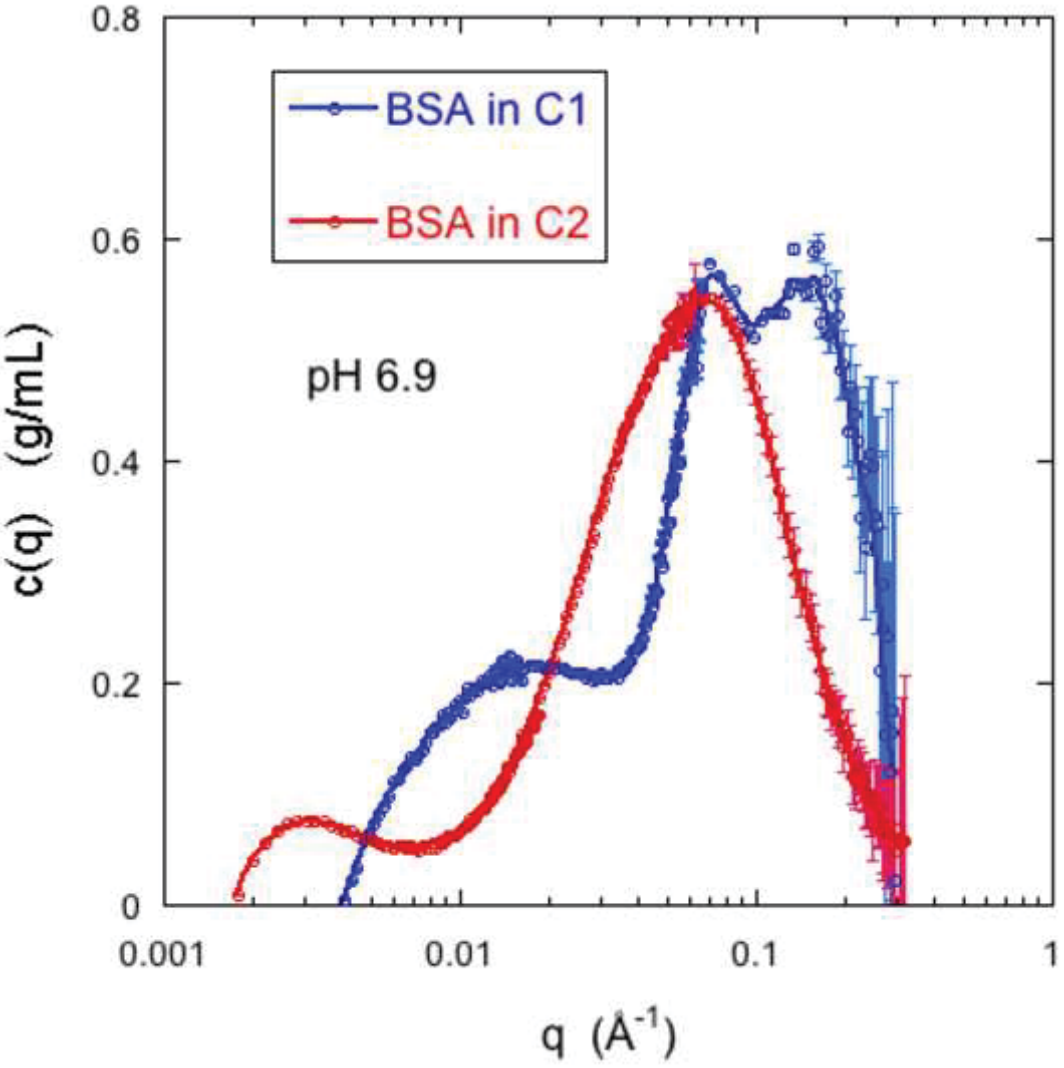

Supplementary Material

Click here to download Supplementary Material: SUPPLEMENTARY_revised to submit.docx